
# Frequency of boulders transport during large floods in hyperarid areas using paleoflood analysis – An example from the Negev Desert, Israel

Noam Greenbaum, Uri Schwartz, Paul Carling, Nati Bergman, Amit Mushkin, Rami Zituni, Rafi Halevi, Gerardo Benito, Naomi Porat

PII: S0012-8252(19)30622-1

DOI: https://doi.org/10.1016/j.earscirev.2020.103086

Reference: EARTH 103086

To appear in: *Earth-Science Reviews*

Received date: 17 September 2019

Revised date: 23 December 2019

Accepted date: 13 January 2020

Please cite this article as: N. Greenbaum, U. Schwartz, P. Carling, et al., Frequency of boulders transport during large floods in hyperarid areas using paleoflood analysis – An example from the Negev Desert, Israel, *Earth-Science Reviews*(2019), https://doi.org/10.1016/j.earscirev.2020.103086

# Frequency of boulders transport during large floods in hyperarid areas using paleoflood analysis – An example from the Negev Desert, Israel

**Noam Greenbaum[1], Uri Schwartz[1], Paul Carling[2], Nati Bergman[1], Amit Mushkin[3], Rami Zituni[1], Rafi Halevi[4], Gerardo Benito[5], Naomi Porat[3]**

[1] University of Haifa, Mt. Carmel, Haifa 3498838, Israel

[2] University of Southampton, Southampton, SO17 1BJ, UK

[3] Geological Survey of Israel, Jerusalem 9692100, Israel

[4] Nehara, Misgav, Israel

[5] Museo Nacional de Ciencias Naturales, CSIC, Madrid 28006, Spain

**Abstract**

Direct measurements of boulder entrainment in desert wadis are not available. The 2004 flood (peak discharge - 470 $m^3 s^{-1}$; recurrence interval - 120 years) in the hyperarid, ungauged Nahal Hatzera ephemeral stream (45 $km^2$), transported and deposited 0.85-1.5 m concrete boulders and slabs detached from infrastructure upstream and natural boulders. EDM and drone air-photographic surveys documented the geometry of the study reach and the location of boulders. Analyses of flood slackwater deposits established a paleoflood record of 23 floods with peak discharges of 200-760 $m^3 s^{-1}$, during the last 600 years. 1-D HEC-RAS hydraulic analysis provided water surface profiles, discharges and hydraulics, long the study reach and velocity, shear stress and stream power for each boulder. MAX program and Pearson 3 distribution were used for flood frequency analysis. Most of the concrete boulders were deposited in the sub-critical backwater of channel constrictions where velocities were 1.5-2.1 m $s^{-1}$. The largest boulders were deposited in super-critical flow where velocity was 8-9.2 m $s^{-1}$. The alluvial channel enables to transport these concrete boulders, reflecting the unstable, active sandy layer of the channel bed over which the boulders moved. The maximum

flood shear stress and stream power characterize medium-large floods with return period of 20-120 years and not for the largest floods, as expected. Boulders <2.1 m and weighing <15 tonnes can be transported at least once in 120 years. The shear stress and stream power indicate that the moderate-large floods are the most geomorphically effective floods rather than the largest floods in Nahal Hatzera basin. Nevertheless, the 'geomorphic effectiveness' of the 2004 flood – a typical desert flash flood, was small based on the minor changes along the channel and banks indicating that their resistance thresholds were not exceeded and energy expenditure was mainly on boulders entrainment and transport.

**Key words:** boulders transport; paleoflood hydrology; ungauged catchments; desert flood; flood frequency analysis; shear stress; stream power; geomorphic effectiveness

## 1. Introduction

Estimating the frequency of high magnitude floods, especially in arid areas where hydrological data are scarce or absent, has always caused debate and has been the subject for numerous estimations and interpretations among hydrologists, geologists and engineers (Baker, 2003). The hydrological records of floods are usually short and therefore the return periods assigned to the largest floods are highly dependent on the duration of the record. These limitations leave space for various assumptions, estimates and modelling. Also, the short time window of the measurements rarely records the larger floods. Estimating the hydraulic conditions and frequency of natural boulders transport is even more difficult because the evidence for boulders motion in nature are rare and usually cannot directly related to a specific time, discharge or other hydraulic parameter.

Paleoflood hydrology provides long-term natural records of the magnitude and frequency for the largest past floods, thereby greatly extending the relatively short systematic flood records available from gauging stations (Kochel and Baker, 1982; Baker, 1987; 2003). The method uses the elevations of paleostage indicators (PSIs) such as slackwater deposits (SWDs), driftwood and erosion lines above the channel and age dating. Paleoflood data enable: (a) documentation of the largest floods that occurred in a basin; (b) extension or establishment of hydrological records of hundreds and thousands of years, and; (c) enhancement of the frequency analyses of the flood records by an improved fitting of the probability functions (e.g. Stedinger and Cohn, 1986; Webb et al., 1988; Thorndycraft et al., 2003). Optimal paleoflood data can be obtained from bedrock canyons, where cross sections, the course of the river, and channel gradient are stable (Baker et al., 1979; Patton et al., 1979; Kochel et al., 1982; Ely and Baker, 1985; Baker, 1987; Baker and Kochel, 1988). Slackwater deposits represent the minimum elevation of the high stage of the flood. Ideal paleoflood sites preserve multiple flood SWDs from which paleoflood records can be established. The location and analysis of these stratigraphic records were widely discussed by Baker (1987) and Benito et al. (2003). Paleo-discharge estimates are obtained using the HEC-RAS hydraulic procedure (Hydrologic Engineering Center, 2018). Ages of paleofloods are obtained using: (a) radiocarbon dating of fine organic debris, wood and charcoal which float near the surface of the floodwaters and are deposited at the top of the flood SWD or as driftwood line; (b) Optical Stimulation Luminescence (OSL) for the fine sandy fraction of these suspended sediments. The flood frequency analysis can use several programs, which combine and integrate various types of hydrological records including systematic, historical, and paleoflood. A review of various methods for incorporating paleoflood

data and other non-systematic information into FFA and risk assessment, was provided by Frances (2004) and Benito et al. (2004).

In the Colorado River, large floods were found to be much more frequent than indicated by estimations based on frequency analysis of the systematic gauge record alone, indicating that gauged records are biased towards low flows. Therefore, the average long-term frequency analysis greatly underestimates the frequencies of extreme floods (Greenbaum et al. 2014).

In the Negev desert, hydrological data are scarce or absent. Extreme hydrological events usually are documented by various public agencies, such as the Soil Erosion Research Station (SERS) and the Israel Hydrological Service (IHS) (Ben-Zvi and Kornitz, 1975; Polak, 1988; Garti et al., 1994; 1998; Greenbaum et al. 1998; Dayan et al., 2001; Ziv et al., 2004; Greenbaum and Schwartz, 2005; Arazi and Getker, 2006; Greenbaum et al, 2010). For such extreme events, determinations of frequencies are problematic. For example, a wide range of probabilities were assigned to floods in medium-sized (10-100 $km^2$) tributaries to the Dead Sea in the northeastern Negev desert, that occurred during the 29 October 2004 rainstorm (Greenbaum et al., 2010; Fig. 1). This problem was related to: (a) The variable accuracy of the short and discontinuous hydrological records; (b) The small number of hydrometric stations, and; (c) The statistical procedures employed (Greenbaum, 2007).

Long paleoflood records, which exceed hundreds to thousands of years, were reconstructed in the larger basins of the Negev - Nahal Zin, Nahal Paran, and Nahal Neqarot (Greenbaum et al., 2006). Nevertheless, even smaller basins in the region preserve paleoflood evidence. The paleo-peak discharges in the Negev Desert are usually two to three times larger than the largest flood in the gauged record.

Boulder bars may serve as evidence for past extreme events. Nevertheless, direct measurements of boulder entrainment in desert wadis are not available. Consequently, recourse is made to theoretical perspectives (Lamb et al., 2015; van Rijn, 2019) mediated by small-scale experimental data (Carling and Tinkler, 1998; Carling et al., 2002) and field observations from shallow high-velocity flows (e.g. Costa, 1983; Williams, 1983; Komar, 1987). Variability in the force required to entrain a boulder largely is related to the degree of particle protrusion within the bed such that beds can be regarded as loose or compacted. Compaction of clasts in a bed tends to be due to protracted flows having rearranged boulders such that few boulders protrude into the flow where they might be readily entrained by a later high discharge. In contrast, boulders deposited rapidly on the surface of a stable bed tend to stabilize in prominent positions. Despite the inevitable uncertainty noted above, consideration of empirical data demonstrates that the variability between loose and compacted bed conditions fall within prescribed theoretical limits (Carling, in press). In this way, the stability of boulders recorded from this study can be considered in conjunction with flood flow modelling.

## 2. Study area

### 2.1 Makhtesh Hatzera Erosion Cirque

"Makhtesh" ("crater" in Hebrew) Hatzera is one of four erosion cirques in the Negev Desert (Israel) and Sinai (Egypt). Makhtesh Hatzera Erosion Cirque (MHEC) is a deep, oval shaped depression 5 x 7 km in size, surrounded by 300-400 m high cliffs (Fig. 1). It is situated, similar to the other erosional cirques, at the crest of a southwest – northeast, asymmetric anticline that forms a prominent topographic ridge where the southeastern flanks of the anticlines are steeper ($60^{o}$-$90^{o}$) in comparison with the northwestern flanks

($6^o$-$15^o$) (Zilberman, 2000). The geology of the structure is composed of hard upper Cretaceous carbonate rocks exposed at the top of the cliffs overlying relatively soft lower Cretaceous sandstone. At the bottom, along the axis of the anticline, older Jurassic dolomite and marls are exposed. The MHEC has one outlet through a deep gorge incised in the steeply inclined southeastern flank, which is the only opening for the drainage system that drains the MHEC. The formation stages of the "Makhtesh"s are summarized by Zilberman (2000).

**2.2 Nahal Hatzera catchment**

Nahal Hatzera ephemeral stream catchment (45 $km^2$) which drains the MHEC, is a tributary to the major stream of Nahal Zin (1400 $km^2$), which drains into the Dead Sea (Fig. 1). The catchment of Nahal Hatzera comprises of two parts (Fig. 2): (a) A Pliocene-Pleistocene, oval shaped, sub-basin inside the erosion cirque (30 $km^2$), which drains the steep slopes and the bottom of the cirque to the southeast, towards the outlet of the MHEC; (b) An older, Miocene-Pliocene drainage system outside the cirque (15 $km^2$), with a northwest flow direction towards the Mediterranean, which was reversed and captured to the southeast by the Dead Sea Rift during the Plio-Pleistocene (Fig. 2). The drainage network of the sub-basin within the cirque is dense (drainage density – 5.3 $km/km^2$) and steep (weighted average gradient – 6.12%), whereas for the sub-basin outside the cirque it is relatively sparse (drainage density - 2.9 $km/km^2$) and the gradient is moderate (weighted average gradient 2.36%) (Fig. 2). The exposed bedrock at the bottom of the MHEC is composed of sandstone and some dolomite, but most of its area is covered by Pleistocene to Holocene conglomerates in the form of abandoned gravelly alluvial terraces. These terraces were mapped and IRSL dated to <630 ka (Plakht, 2003) and between 334±36 and 45.6±3.3 ka by Fruchter et al., (2011) using OSL abandonment

ages and $^{10}$Be exposure ages. These alluvial surfaces are topped by well-developed desert pavement underlain by Reg soils, which are relatively impermeable and generate runoff. Outside the cirque, the bedrock is composed of carbonate rocks at the upper reaches and mainly Miocene conglomerates, sandstone and sands at the center.

The similar distance – about 7 km from the escarpment to the outlet, for most tributaries within the MHEC due to its oval shape (Fig. 2), determines similar tributary gradients resulting in similar concentration times for floods generated by rainstorms that cover the catchment. Therefore, the floods at the outlet of the MHEC are characterized by high peak and short duration.

Due to the absence of gauging station along the channel of Nahal Hatzera the hydrological data are scarce. Large observed floods occurred in 1994, 2004 and 2018 (Table 1). Peak discharges were estimated using slope-area method. The largest documented flood (October 2004) had a peak discharge of 580-600 $m^3 s^{-1}$ (Greenbaum and Schwartz 2005; Getker and Arazi, 2006; Greenbaum et al., 2010). For the period 1964-1994 (30 years) Greenbaum and Lekach (1997) reconstructed evidence for 19 floods in a small tributary of Nahal Hatzera (7.3 $km^2$) - an average frequency of one flood per 1.6 years.

### 2.3 **The October 2004 rainstorm and floods**

An Active Red Sea Trough system (ARST) (Kahana et al., 2002; Dayan and Morin, 2006), with a cold upper trough, high moisture content, and relatively high temperatures at low levels, caused instability and severe convection that generated an intensive rainstorm on 29 October 2004.

Rainfall characteristics

Rainfall analysis was performed by Getker and Arazi (2006). Measured storm rainfall amounts increased from west to east up to a maximum of 74 mm in Sedom (Fig. 3). The Sedom value was the largest on record since 1938, and had a probability of about 1% (Getker and Arzi, 2006). The largest measured 10-minute rainfall amount at the Sedom rain gauge was about 30 mm (intensity of 175 mm $hr^{-1}$) with a probability of 0.5-1%. Based on radar images, the core of the storm located at the northeastern Negev lasted >2 hours (Fig. 3), during which it moved eastward. The storm covered the southwestern tributaries of Dead Sea including Nahal Hatzera and other tributaries of the lower Nahal Zin (Greenbaum et al., 2010; Fig. 1). Reconstructed rainfall amounts for the MHEC using non-calibrated rainfall radar data estimated the storm rainfall amount at 60-70 mm within about 2 hours (Fig. 3).

Flood characteristics, magnitudes and frequencies

The spatial and temporal distribution of the floods generated by this rainstorm varied greatly. Large floods with estimated exceedance probabilities of 1% were generated in catchments of all sizes. The flows had "flashy" characteristics, typical of autumn ARST-generated events. Extreme large floods were generated in medium-sized (10–100 $km^2$) basins (Fig. 1), with specific peak discharges up to 18 $m^3 s^{-1} km^{-2}$ (Getker and Arazi, 2006). The calculated probabilities for the floods of the October 2004 rainstorm vary between about 1% at the center of the storm to 20% at its periphery. Some of these magnitudes exceeded the envelope curve of the Negev and Dead Sea region (Greenbaum et al. 2010). Nahal Zin, the largest basin in the region (1400 $km^2$; Fig. 1), generated the largest flood on record (1935-2019; 84 years), with a peak discharge of about 1280 $m^3 s^{-1}$ (estimated exceedance probability of 1%), even though that the actual contributing area was about 600 $km^2$ only (43% of the total drainage area). Each of its tributaries also generated the largest flood on record (Fig. 1; Greenbaum et al., 2010).

The October 2004 flood in Nahal Hatzera ephemeral stream

Based on the radar data and on our field survey, the October 2004 rainstorm entirely covered the drainage basin of Nahal Hatzera. The storm generated extremely large floods in all the tributaries and their waves combined near the outlet of basin to an estimated peak discharge of 580 $m^3 s^{-1}$ using slope-area method (specific peak discharge of about 12.9 $m^3 s^{-1} km^{-1}$; Getker and Arazi, 2006). Concentration time was calculated using the Soil Erosion Research Station (SERS) formula – a local version of the Kirpich formula, to between 60-70 minutes. A peak discharge of about 600 $m^3 s^{-1}$ was assigned downstream were drainage area is larger (50 $km^2$, Greenbaum and Schwartz, 2005). This peak discharge exceeded the envelope curve of measured floods in the Negev, and had an estimated exceedance probability of about 1% (Getker and Arazi, 2006; Greenbaum et al., 2010). Water stage of the flood was based on the clear driftwood line along the entire reach, which in places, exceeded an elevation of 8 m (Fig. 5a) (Greenbaum and Schwartz, 2005; Getker and Arazi, 2006).

**2.4 Study site**

The study reach is located at the outlet of the MHAC (Fig. 4). It is composed of three segments from downstream to upstream: (A) an alluvial segment about 140 m long downstream of the gorge covered with large boulders, where the channel widens to about 80 m and gradient is about 0.014 (Fig. 4). (B) an intermediate segment in the form of narrow bedrock gorge – 160 m long and up to 12 m wide only, a gradient of about 0.043 composed of hard carbonate rocks with nearly vertical walls (Figs. 4, 5a); (C) a curved alluvial segment 200 m long, with a relative wide cross section (70 m) and a gradient of about 0.031. A large boulder bar is attached to the right bank of the active channel, with a secondary channel along the other side of the bar, active in high floods

only (Figs. 4, 5b, 8). A British Mandate road through the gorge, leading to groundwater wells within the cirque, was constructed in the 1930s, but was completely swept away by the 1994 flood (230 $m^3 s^{-1}$; Greenbaum and Lekach, 1997). A concrete road was constructed in 1998 by filling the original channel with about 2m-thick layer of concrete (Figs. 4, 5a). The concrete road serves as the present channel for segment B and due to the low roughness and the steep gradient - 0.043 the road is self-cleaning with no deposition of sediments during floods. In segments A and C - the outlet and inlet of the gorge, the 2004 flood deposited large boulders. Trapped driftwood, large concrete boulders and slabs detached from a small pump structure, wall, and road surface upstream and other indicators helped to identify transported versus stable boulders (Table 2). Boulder survey was conducted immediately after the flood along the upper and lower segments to define the largest boulders transported during the flood (Figs. 4, 5b).

## 3. Methods

### 3.1 Hydraulic methods

The HEC-RAS hydraulic model (Hydrologic Engineering Center, 2010), was used to generate water surface profiles, using step-backwater calculations for various discharge values (O'Connor and Webb, 1988; Webb and Jarrett, 2002). Comparing the elevations of the SWDs and PSIs with the computed elevations provides an estimation of the minimum peak stage. Differences between the elevation of SWDs and driftwood lines and gauged discharges in Nahal Zin, for example, indicate that the elevation of the SWDs is lower than the actual peak stage by 50-70 cm for large floods (Greenbaum et al., 2000). Therefore, paleoflood hydrology is a conservative method, which

underestimates peak discharges and the calculated values should be treated as minima (Kochel et al., 1982; Baker, 1987).

Water surface profiles for large floods in relatively narrow bedrock-controlled streams are typically subcritical (e.g., Ely and Baker, 1985; O'Connor et al., 1986; Baker, 1987; Partridge and Baker, 1987; O'Connor and Webb, 1988; Wohl, 1998; Greenbaum et al., 2000). Supercritical conditions are reached rarely where the channel gradient increases abruptly, such as large cataracts and rapids, or downstream of abrupt constrictions (Greenbaum, 2007), depending on the discharge. Other uncertainties for paleoflood hydrology discharge calculations (O'Connor et al., 1994) include: (a) flow conditions downstream of the study reach and their effect on the local surface profiles; (b) values for the energy loss coefficients, and; (c) channel geometry during peak flow stages. Inaccuracy in the discharge estimations may also result from the selected hydraulic roughness coefficient; studies of Manning's ***n*** choice for calculating very large discharges in narrow, deep bedrock canyons show low sensitivity (O'Connor and Webb, 1988; Wohl, 1998; Greenbaum et al., 2014). The HEC-RAS simulations enabled also to extract hydraulic parameters such as velocity, shear stress and stream power for each cross-section.

### 3.2 Remote sensing

High-resolution (5 cm/pixel) orthophotographs and topography were produced from drone-based photography (DJI Mavic2 zoom) processed through the Agisoft Metashape 1.5 software package. The cross sections were located over the orthophotographs to show the morphology of the study reach and cross sections.

### 3.3 Boulder measurements

The three-axis geometry of the largest concrete boulders, slabs and natural boulders and their location within the bar and in the cross sections, were surveyed and documented. The concrete boulders received numbers. The surveyed boulder population included also large boulders that were considered immobile (Table 2). The boulders locations in the cross-sections serves for calculations of the hydraulic parameters relevant to transport and deposition.

### 3.4 Optical Stimulated Luminescence (OSL)

Optically stimulated luminescence (OSL) dates the last exposure of quartz grains to sunlight and assumes to provide the age of the transporting flood.

Samples for OSL were collected from sediment sections in the profiles of the gorge cave, the gorge section and the SWD section (Fig. 6). To avoid exposure to light, samples were taken under cover either by a hand-held cylindrical auger or by scraping sediment beneath a black out sheet into light tight bag. At least 10 cm were removed from the exposure surface prior to sampling. An additional sample was collected from the same locations for dose rate evaluations.

Quartz in the size range of 90-125 μm was extracted using routine laboratory methods (Table 3; Faershtein et al., 2016). The De values were measured using the OSL signal and the single aliquot regenerative dose (SAR) protocol. Preliminary measurements showed a very large scatter of De values within samples, most like the result of partial bleaching of the quartz grains during the short transport distance. To identify the youngest, best bleached population of grains, 41 to 65 1-mm aliquots (with about 50 grains on the disc) were measured. The Minimum Age Model (MAM) or the Finite

Mixture Model (FMM) were used to isolate the youngest age population. For the latter, the youngest component comprising >10% of the measurements was selected. Additionally, for one sample 500 single grains were measured (protocol following Porat et al., 2006), and processed using the FMM.

Dose rates were calculated from the concentration of the radioactive elements measured by ICP-MS (U and Th) or ICP-OES (K). Cosmic dose rates were evaluated from current burial depths and the moisture content was estimated at 2±1%.

### 3.5 Radiocarbon dating

Three coal and wood samples, all from stratigraphic context, were sent for radiocarbon analyses to the AMS laboratory at the University of Arizona (Table 4).

## 4. Results

### 4.1 Paleoflood Chronology

The dating in the study site uses both OSL and radiocarbon methods.

OSL dates the last exposure of quartz grains to sunlight before burial and therefore is assumed to provide the date of the flood. The OSL ages, based on small (1mm) aliquots and either the FMM or MAM, provide ages in the range of 4-14 ka (Table 3). For each of the sections, while in stratigraphic order, the ages are much older than the corresponding radiocarbon dates (see Fig. 6). The single grain age for sample MKT-42 was calculated using the youngest component identified by the FMM and is based on only 3% of the grains, i.e two of the 64 accepted grains. Even that age, 2,200 years (200 BC), is much older than the radiocarbon date from that unit, 1689-1926 AD, so even single grain measurements cannot resolve the poor bleaching of the grains. Thus, it

appears that during the rapid and short transport, very few of the grains, if any at all, were sufficiently bleached with regard to the OSL signal, and all OSL ages should be treated as maximum ages.

Radiocarbon - The radiocarbon dates range between 1445-1634 AD and 1689-1926 AD (Table 4), indicating floods in the past six centuries, and as mentioned, are much younger than the OSL ages (Fig. 6). Samples for radiocarbon were taken from within the units, from redeposited twigs and charcoal, and there is no reason to suspect contamination with young, sub-modern material.

Field evidence suggests that the SWDs and other flood-related sediments, are very young: (a) the sediments are loose with no evidence for cementation or other pedogenic processes expected for sediments that have been at the surface for many thousands of years; (b) it is unlikely that such vulnerable sediments survived thousands of years of large and eroding floods; therefore, the quality of preservation of these sections suggests a younger age; (c) The regional paleohydrological context of the northeastern Negev shows that such old flood deposits were not found in medium-size catchments, only those of the past several hundred years (Greenbaum et al., 2006); (d) large floods with similar specific discharges were already documented in other catchments in the region. As the geomorphic settings dictate short transport distances with high suspended load (which may also occur at night), poor bleaching of the OSL signal is very likely. We conclude therefore, that in the present study, the radiocarbon dates are more reliable than the OSL ages.

**4.2 Paleoflood sites and Stratigraphy**

The paleohydrological data for Nahal Hatzera, are derived from four sites along the upper and middle sections (Figs. 4, 6, Table 1). The SWDs at these sites were documented, analyzed and systematically OSL dated. Radiocarbon dating was applied to samples from units where organic material was found. The sites contains 3-8 sedimentary units each. Floods with similar age and discharge in different stratigraphic sections were assumed to represent the same flood. The driftwood of the 2004 flood and the 2018 flood along the study reach helps with the calibration of the HEC-RAS hydraulic analysis.

Site MK-1 - This 3.3 m SWD section is an overbank deposit located upstream of the inlet to the gorge at the left bank (Figs. 4, 6a). The top of the section is 7.4 m meters above present channel bed. It includes six sandy well-bedded sedimentary units. The thickness of the units vary from – 10 to 110 cm. Units 2, 4 and 6 were OSL dated to 13.9±1.4, 12.0±0.7, and 8.0±0.7 ka, respectively. Unit 6 was also radiocarbon dated to 1489-1644 AD.

Site MK-2 - This 1.9 m SWD section was deposited in a cave just next to and downstream of the MK-1 site (Figs. 4, 6b). The top of the section is 4.9 m above present channel bed. The units are 15-60 cm thick and includes five sandy, well-bedded sedimentary units. Unit 4 was radiocarbon dated to 1445-1634 AD, whereas unit 5 was OSL dated to 4.5±0.4 ka.

Site MK-3 – This overbank site is located at the gorge among large boulders derived from the slope at a local expansion on the right bank (Figs. 4, 6c). The SWD section is 1 m thick, at the right bank, about 9 m above channel bed and contain three sedimentary units, 25-40 cm thick. The sedimentary units are composed of well-bedded sand. Unit 2 was both OSL and radiocarbon dated to 4.8±0.6 ka and 1689-1926 AD, respectively.

Site MK-4 –This site, is located in a small cave at the outlet of the gorge (Figs. 4, 6d) was documented by Greenbaum (1996). It is 75 cm thick and includes eight sedimentary events. The elevation above the natural channel bed is 5.9 m. The sedimentary units are 5-15cm thick, and are composed of well-bedded sand and silt. Units 2 and 7 were OSL dated to 10.5±0.8 and 7.8±0.7 ka, respectively. HEC-2 water surface profiles that were iterated after the 1994 flood when the bedrock channel at the gorge was completely exposed (Fig. 5e), provided peak discharges of 250-300 $m^3$ $s^{-1}$ for this section (Greenbaum, 1996).

**4.3 Boulders survey**

Results of the largest boulders survey at the inlet to the gorge where velocity dramatically decreases, and a large boulder bar deposited, are presented in Table 2. This natural boulder bar predates the 2004 flood as indicated from British (Survey of Palestine, 1946) air-photographs, but the 2004 flood, deposited new boulder lobes over the boulder bar, which in addition to natural boulders, included concrete boulders and slabs detached from infra-structures upstream. The concrete boulders, trapped driftwood by boulders, natural boulders deposited over or imbricated with concrete boulders serve as indicators for mobilization by the 2004 flood. The field survey, documented the largest boulders and blocks in the upper segment, and classified them into four groups, 6-9 boulders in each group (Table 2, Fig. 5b): (a) Immobile, natural, very large limestone blocks with angular edges, that are not oriented to flow direction and are sourced from rockfalls from the canyon walls in the immediate locations. Some of these boulders faces are covered with lichen and desert varnish; (b) Mobile angular concrete blocks and slabs that were eroded into the flow and which rolled, or slid over the channel-bed (Figs. 5b, 5d, 8). Smaller boulders were deposited over the boulder bar

(Figs. 5b, 5c, 8). Their sizes and volumes overlaps the range of natural mobile boulders; (c) Mobile natural, rounded, smooth blocks and boulders with no sharp edges, were often located flow-transverse. Imbrication is common in the case of slabs. They are composed of limestone, dolomite and sandstone sourced from the upper parts of the basin; (d) Possibly mobile natural boulders are less rounded, more rough, sometimes flow-transverse and show indication of rolling. The equivalent cuboid and ellipsoid volumes of the boulders were calculated (Table 2). The intermediate boulders sizes of mobile natural and concrete boulders ranges between 0.6-2.1 m and the maximum equivalent cuboid volume ranges between 5.25-6.41 $m^3$ (2.5 $m^3$ in average). The weight of the concrete boulders ranges between about 0.82-15.56 tonnes (average 5.96 tonnes) (Table 5). In contrast, immobile blocks are much larger and have an average equivalent cuboid volume of 32.7 $m^3$. The largest concrete boulders were found at or nearby the channel bed, whereas the smaller concrete boulders were found on the boulder bar some of which imbricated with natural boulders of similar sizes. Several concrete cobbles of 20-30 cm in size were deposited on the slopes of the side-walls of the gorge, 1-2 m below the high-water marks of the flood throughout the gorge. The mobile and possibly-mobile boulders have no lichens or desert varnish cover.

**4.4 HEC-RAS simulations**

The study site has complex hydraulics because of the channel irregularities such as: (a) Abrupt expansion and constrictions; (b) transitions from alluvial sections to a bedrock gorge, and; (c) changes in gradient; (d) curvatures.

We used 1-D, HEC-RAS (Hydrologic Engineering Center, 2018) version 5.0.5 program with a mixed flow regime. Twenty-eight cross sections were surveyed along the 500 m

reach (Figs. 4, 7) - about 18 m of each other, in average. Manning ***n*** was estimated for banks and channel for each cross section. For peak discharge calculations we reconstructed two types of channels: (a) pre-2004 natural bedrock channel for the paleofloods which had flowed over the natural bedrock channel (Fig. 7a) and; (b) a 2-meter higher, post-1994 "concrete channel" which served as the channel bed for the 2004 flood (Fig. 7b). Water surface profiles between 100 and 700 $m^3s^{-1}$ were constructed along the study reach for peak discharge determinations. Boundary conditions were set for critical depth. The determination of the peak discharge of the 2004 flood is based on the clear high water marks (HWMs) in the form of clear driftwood line along the entire reach. After the 2004 flood the upper segment (segment C) of the study reach has undergone dirt road construction, which elevated the active channel by up to 2m. Since our survey was conducted in 2016, it provided lower peak discharges for the 2004 flood along this reach (Fig. 7b). Therefore, our peak discharge calculations were performed along the gorge (segment B), where the concrete channel-base and rocky banks are stable. A peak discharge of 470 $m^3 s^{-1}$ was fitted consistently to the 2004 HWMs throughout the gorge and was projected upstream to the disturbed segment C using the actual HWMs and by artificially lowering the channel level until adjustment to 470 $m^3 s^{-1}$ was achieved. For the estimations of the paleoflood peak discharges, the natural bedrock channel was reconstructed by lowering the present concrete channel level by 2 meters – the thickness of the concrete filling, along the gorge (Fig. 7a). The continuous projected profile and the channel geometry along the upper segment (segment C) were assumed to represent the undisturbed, pre-road construction, natural conditions.

The present study employed two sets of roughness coefficients to produce various hydraulic scenarios and to choose the best fit to the HWMs: (a) Manning ***n*** values that

were estimated in the field and ranged between 0.02 to 0.085; (b) Manning ***n*** values that were preset for the three segments of the study reach A, B and C, to 0.06, 0.02 and 0.08, respectively. A wide range of contraction-expansion coefficients were tested: 0,0; 0,0.5; 0.1,0.1; 0,0.3; 0.1,0.3, and 0.3,0.8 in order to define the best fit. Finally, we adopted the default values - 0.1,0.3 throughout the study reach. The HEC-RAS simulations show three locations of back-water development along the channel at the gorge due to abrupt local channel constrictions at the 170, 220 and 305 meters markers along the channel, which causes high backwater levels (Fig. 7) separated by short reaches of accelerated flow where water levels fell abruptly. The flow at these constrictions was supercritical with velocities of up to 9.2 m $s^{-1}$.

**4.5 Flood Frequency Analysis (FFA)**

For the FFA we used only floods with peak discharges >200 $m^3$ $s^{-1}$ and radiocarbon ages (25 floods, Table 1). The actual data set is composed of: (a) Radiocarbon dated floods and younger floods based on the stratigraphy; (b) Based on the continuous and the ordered OSL stratigraphy, we used the relative differences in ages between OSL dated floods within the stratigraphic sections, to fit a relative "radiocarbon age" to OSL dated floods (c) The two observed floods of 1994 AD and 2004 AD. Together, these data provide a paleoflood record of 10 floods for the FFA.

The FFA was performed based on the paleoflood data (discharge and $C^{14}$-timing) and the two observed floods for which exact discharges and dates are known. Development of robust flood flow frequency ideally requires multiple data sets involving paleoflood data, measured annual peak discharges and/or regional flood quantile regression equations (Tasker and Stedinger, 1989; England Jr et al., 2019; ). The lack of gauged data in the present study is a clear shortcoming, but in arid regions annual flood series

include many 'zero flows' or very small floods for most of the monitoring time period. The dominance of small floods (e.g. annually) in gauged records tend to skew FFAs and therefore, most statistical procedures recommend to eliminate small floods because they are not relevant to estimating the frequency distribution of the largest floods (National Research Council, 1988; Klemeš, 2000). In the present study, our purpose is to obtain the best possible agreement between the observed and estimated frequency distributions at the upper tail of the frequency curve (AEPs 1% and smaller). The frequency analysis was performed using the Maximum Likelihood Estimation Method (MLE) MAX program (Stedinger et al. 1988), which is most efficient to properly utilize non-systematic paleoflood data and handle censored flood data focusing on the frequency of large floods. The MLE method calculates the values of the parameters of the distribution function that maximize the probability for obtaining the set of the n values of the observed sample (Stedinger and Cohn, 1986). The MAX program was used to estimate parameters of several probability distributions including: (a) normal (b) lognormal (c) Pearson type 3 (d) log-Pearson type 3 (Fig. 9; table 6).

A critical assumption is that all the floods above specific discharge thresholds are recorded in the stratigraphy. The thresholds are determined by the elevation of the base of the SWDs traps, where only the floods that exceed this threshold are recorded and smaller floods are not. For this analysis, the key data were the exact discharge calculated for the two observed floods, the eight largest floods over the last 770 years (MK1 and MK3 sites), for which the discharge was specified, and three upper bounds (discharge thresholds). The upper bounds were defined by the elevation and time interval of the MK1 and MK3 paleoflood sites (440 and 380 $m^3s^{-1}$), and a perception threshold (230 $m^3s^{-1}$) for observed floods over the last 25 years. The exact date of each flood is unknown, but for practical purposes, each palaeoflood unit was assigned a central

radiocarbon age or interpolated year. Note that the number of events over the time interval affects the frequency and not the exact year. Plotting positions of paleoflood data were assigned using the Weibull equation (Fig. 9). In this analysis, the best optimization for the statistical parameters was obtained for the Normal and Pearson type III distributions. The set of logarithmic probability distributions provided very high results for the small quantiles as well as for the high quantiles in relation to the paleoflood plotting positions (Fig. 9).

## 5. Discussion

### 5.1 Paleoflood record

Altogether, 23 paleofloods were reconstructed at the four sites with peak discharges ranging between 200 and 760 $m^3 s^{-1}$ (Table 1, Figs. 4, 7a). At site MK1, six paleofloods were reconstructed with peak discharges between 400 and 550 $m^3 s^{-1}$ (Fig. 6a); site MK2 – five floods with peak discharges between 200 and 290 $m^3 s^{-1}$ (Fig. 6b); site MK3 – 3 floods with peak discharges between 380 and 430 $m^3 s^{-1}$ (Fig. 6c); MK4 – 8 floods with peak discharges between 250 and 300 $m^3 s^{-1}$ (Fig. 6d; Greenbaum, 1996). Flood units with similar reconstructed peak discharge and age, were assumed to represent the same flood, especially for the frequency analysis. In addition, three large floods with peak discharges between 130 and 470 $m^3 s^{-1}$, which occurred during the last 25 years, were documented. The 2004 flood was assigned a peak discharge of 470 $m^3 s^{-1}$. Previous peak discharge estimations for the same flood yielded about 580 and 600 $m^3 s^{-1}$, but these values were calculated in various sites with different drainage areas using slope-area method, which usually provides over-estimations (Greenbaum et al., 2014). According to the frequency analysis, the largest observed floods of 230 and 470 $m^3 s^{-1}$ are associated with recurrence intervals of 25 and 120 years (Fig. 9, Table 6). The 2004-

flood in Nahal Hatzera was previously assigned a similar frequency of about 100 years and the 2004-rainstorm a frequency of 50-100 years (Getker and Arazi, 2006; Greenbaum et al., 2010). The largest paleoflood (760 $m^3s^{-1}$) is associated with a recurrence interval ranging between 380 to 800 years, based on the Log-Person type 3 and Pearson type 3 distributions, respectively.

**5.2 Boulders transport**

A large number of smaller concrete boulders had been found downstream of the surveyed sections indicating that they were transported through the gorge (segment b) and deposited in the downstream alluvial reach (segment a; Fig. 4), but no boulders were found within the gorge. The absence of boulders in the gorge largely is related to the high velocities along the gorge due to the smooth concrete bed, the low roughness of the rock banks and the steep gradient. Most large boulders were deposited within the contracting reach at the upper end of the surveyed sections and the deposition of these boulders is considered below.

Within Table 2, boulders are grouped according to a qualitative field assessment of the probability of entrainment in the 2004 flood. The 'mobile natural boulders' have a similar size range as the 'concrete blocks and slabs' which were definitely entrained and transported during the event. Consequently, the conditions for entrainment and dis-entrainment of natural mobile boulders are considered using the concrete block data (Table 5). The hydraulic conditions related to the break-up of the concrete road upstream of the study sections are unknown, but complex (Graham, 1998) and probably include under-mining and hydraulic jacking of the concrete slab until it fractured. Fractured blocks would likely flip over due to fluctuating forces, then slide downstream across any

intact concrete road surface that still persisted and then roll over the alluvial bed upstream of the study reach.

For the sandy alluvial bed upstream of the study reach, Greenbaum et al. (2009) calculated the maximum shear stresses (250-900 N $m^{-2}$) available to transport a range of concrete boulders sizes (0.85-1.45 m) and the three largest mobile boulders found in the boulder bar to derived the entrainment curve (continuous dark line) depicted in Fig. 10. The two largest boulders in the current study (Boulders 1 & 2; Table 5) plot on the function proposed by Greenbaum et al. (2009) which reflects the consistency of the hydraulic computations of Greenbaum et al. (2009) and the current hydraulic reconstructions. Note that boulders 1 and 2 are deposited at the downstream end of the sandy alluvial reach immediately upstream of the hydraulic jump (Fig. 7b). The curve of Greenbaum et al. (2009) falls below the entrainment curves proposed by Baker & Ritter (1977) and Costa (1983). The curve of Costa has been found to represent entrainment from relatively compact beds whereas, in contrast, the Greenbaum et al. (2009) function is not inconsistent with the minimum entrainment function proposed by Williams (1983) for an underloose bed; this is reflecting the unstable, active sandy layer of the channel bed over which the boulders moved.

However, it should be noted that the mobile boulders (Tables 2 & 5) were probably deposited on the falling limb of the flood and actually represent conditions of dis-entrainment, rather than entrainment, as is considered below. Note that all the concrete boulders in this reach are located close to an hydraulic jump that developed in the flow due to the contraction of the reach as the gorge is approached. Acceleration of supercritical flow occurred from +460m (Fig. 7b) as flow shallows to only 0.7m deep at +390m. At this point, a hydraulic jump occurs followed by a steep backwater from +390m to +310m. Concomitantly, the Froude number decreases rapidly from c. 2 at the

location of boulder 1, to subcritical at boulder 4, and continues to decrease as the backwater curve develops to the location of boulder 8 (Table 5; Fig. 7b). Evidently, all the concrete boulders were dis-entrained at the hydraulic jump (boulders 1 and 2 just upstream) with the remainder coming to rest in the developing backwater (boulders 4, 6, 7, 7a, 8 and 9; Fig. 7b). For the remainder, the associated shear stresses are low (Table 5; Fig. 10); the data plotting below the curve proposed by O'Connor (1993). In fact the O'Connor function represents a dis-entrainment curve (Carling, this volume) at which point entrained boulders are very rapidly deposited, and also reflects the fact that, once entrained at fairly high shear stress (e.g. Costa function), boulders can continue to move for relatively low shear stresses.

O'Connor (1993) emphasized that, in a range of published studies, there are large differences between the threshold values calculated, especially for depositional sites where velocity can reduce abruptly, and therefore the assumption of uniform flow conditions is invalid. Nonetheless, the large differences in velocity, shear stress and stream power within each cross-section (Fig. 8, Table 5) encompass the wide spatial variability in transport and deposition conditions. For example, during the 2004 flood, deposition may have occurred towards one side of the channel where local velocity reduced, whereas at the same time, in another part of the cross-section, transport of similar boulder sizes, may have continued. Most of the concrete boulders B4-B9 (Table 5) were deposited in the developing sub-critical backwater where velocities were 1.5-2.1 m $s^{-1}$. The largest boulders 1 and 2 (Table 5) were deposited in super-critical flow where velocity was 8-9.2 m $s^{-1}$. Boulder B7 is much larger than boulder B6 (Fig. 8), but both may have been deposited at the same time due to the different flow conditions (water depth, roughness, velocity, shear stress and stream power) associated with the rapid spatial change in flow conditions through the hydraulic jump. Therefore, although

deposition is site-specific, related to the local hydraulic conditions, careful analysis can produce interpretable results, as here in the case of the hydraulic jump.

Table 7 shows that maximum velocity (9.0-9.8 m $s^{-1}$), maximum shear stress (437-507 N $m^{-2}$) and maximum stream power (4020-4972 N $m^{-1}$ $s^{-1}$), were obtained for the medium-large floods – 200-470 $m^3$ $s^{-1}$. These large values are related to the geometry of the channel, i.e. the constriction of the gorge, where the larger the flood the deeper and greater the backwater "reservoir" and the longer its extension upstream. This backwater reduces water velocity and flow energy indicating that the maximum potential flood effectivity at the present site is obtained for medium-large floods with return period of 20-120 years and not for the largest floods, as maybe expected. The 2004 flood falls within this range and therefore was capable of transporting boulders up to 2.1 m (intermediate axis) and weighing up to 15 tonnes.

**5.3 Flood Effectiveness for Desert Channel Change**

The 'geomorphic work' (Wolman and Gerson, 1978) or 'geomorphic effectiveness' (Schumm, 1973; Costa and O'Connor, 1995) of floods is indicated by the magnitude and nature of the changes throughout the channel induced by the power expenditure of the flood. The shape of the 2004-flood hydrograph, and therefore the detailed time-dependent expenditure of power, is unknown. Nevertheless, the Hatzera flood was a typical desert flash flood, characterized by a high-magnitude peak discharge but a short-duration of a few hours (type C, in Costa and O'Connor, 1995). Such floods generate high instantaneous peak stream power values, but given the short duration, the stream power is not sustained through time and so geomorphic change can be small. Therefore, according to the qualitative disruption criteria suggested by Costa and O'Connor (1995), the high-magnitude, short duration 2004-flood had only a small geomorphic impact at

the study site; notably neither major channel incision nor bank erosion were documented because the resistant rocky and well-cemented conglomerate banks limit changes in the drainage system and flow pattern. The absence of a floodplain limits overbank inundation and deposition of fine sediments, rather the available energy was expended entraining and transporting coarse gravel, including large boulders, from upstream reaches of the channel bed, to deposit the boulders in the backwater reach, before evacuating sediment and the concrete road within the narrows, breaking the concrete into slabs. Nonetheless, some localized bank erosion was observed upstream in part of the tributaries.

In the same vein, several studies have demonstrated similar relationships between moderate-magnitude events, sediment transport, and channel shape and form (Wolman and Miller 1960). Baker and Costa (1987) suggested that geomorphic effectiveness of floods depends on the relationship between the local stream power and bank resistance. As noted at Nahal Hatzera, the power expenditure caused a variety of localized impacts ranging from no impact at all to major channel modifications for the same flood. Inbar (2000) analyzed the 1969 flood – the largest observed flood (Recurrence Interval of 100 yr) along the Jordan River and concluded it was a geomorphic effective flood, based on the changes in the channel and the long distance transport of >260 large boulders >1 m. This definition of effectiveness was clearly related to the long duration (144 hours) of the discharge above a threshold of 140 $m^3 s^{-1}$, needed for boulders entrainment and transport. Kale (2007) studied the geomorphic effectiveness of the largest floods in three rivers in India. He found out that the duration of unit stream power needed for significant transport of boulders >0.5 m was between – 40-80 hours. For one of these rivers, Kale and Hire (2004) indicate that smaller short-duration floods of high power were responsible for channel erosion whereas longer duration floods transported up to

70% of the annual suspended sediment load. Lisenby et al. (2018) argue that the relationships between hydraulic causes and geomorphic effectiveness are often complex and non-linear, but nevertheless, are related to the total energy expenditure. Thus, effectiveness (Schumm, 1973) is related to peak power expenditure as well as the total power expenditure, which is mediated by the duration of the event. The Nahal Hatzera flood was effective in-as-much, as new distinct boulder lobes were deposited in the backwater zone upstream of the channel constriction with intervening reaches being largely zones of bed-sediment evacuation rather than significant channel enlargement. Such behaviour has been reported for other steep small catchments (Carling, 1986; Carling & Glaister, 1987). The long-term persistence of the boulder lobes at Nahal Hatzera is highly probable, as the channel has begun to entrench on the left-hand side of the boulder lobes (Fig. 4). Thus, moderate floods will bypass the lobes rather than rework them. Elsewhere, the channel since the flood appears to exhibit a planform very similar to that present before the flood. As the large boulder lobes did not exist before the flood it is reasonable to conclude that a significant geomorphological threshold was exceeded, but the lack of other notable channel adjustments may indicate that the channel is already adjusted to a condition of 'maximum' discharge (e.g. Chorley and Morgan, 1962) defined by the passage of paleofloods prior to 2004. Alternatively, the channel-form, being mostly bedrock-constrained, may be insensitive (Brunsden and Thornes, 1979) to the magnitude of large floods.

The contrast between the presence of new boulder lobes and little other channel change is a good example of 'complex' response (Schumm, 1973) of landscapes to geomorphic drivers. The channel response depends on the power exerted by the flow, the duration of the event and the availability of sediment for potential redeposition and storage. The Nahal Hatzera channel can be viewed as insensitive in-as-much as visually the channel-

form returned to its approximated pre-flood geometry rapidly after a relatively rare flood event, although boulder lobes persist.

In summary, at Nahal Hatzera, during the moderate-large size 2004 flood: (a) surface and channel resistance thresholds were not exceeded; (b) the majority of energy expenditure was on boulder and concrete slab entrainment and transport. (c) the channel is insensitive to large floods.

## 6. Conclusions

Paleoflood hydrology reconstructed a paleoflood record of 23 floods with peak discharges of 200-760 $m^3 s^{-1}$ during the last 600 years, for the ungauged basin of Nahal Hatzera, in the hyperarid Negev Desert. The concrete and imbricated natural boulders deposited during the 2004 flood (470 $m^3 s^{-1}$) provide clear evidence for boulder transport. The FFA indicated that this flood had a return period of about 120 years. The hydraulic analysis provides the hydraulic conditions i.e. velocity, shear stress and stream power for each boulder at its specific location. The results indicate that most of the concrete boulders were deposited in the sub-critical backwater of a channel constriction where velocities were 1.5-2.1 m $s^{-1}$. The largest boulders, were deposited in shallow super-critical flow where velocity was 8-9.2 m $s^{-1}$. For the alluvial bed of the Nahal Hatzera channel, maximum shear stress of 250-900 N $m^{-2}$ are available to transport a range of concrete boulders sizes (0.85-1.5 m), reflecting the unstable, active layer of the channel bed over which the boulders moved. The mobile boulders were deposited on the falling limb of the flood and therefore, represent settling conditions. The FFA analysis and resulting peak discharges provide the following maximum depositional hydraulic values for return periods of 10-1000 years: velocity - 7-10 m $s^{-1}$, shear stress - 300-500

N $m^{-2}$ and stream power - 2500-5000 N $m^{-1}$ $s^{-1}$. The frequency of the 2004-flood, indicates that boulders up to 2.1 m and weighing up to 15 tonnes can be transported at least once in 120 years. The geomorphic effectivity of this typical desert flash flood was small based on the qualitative properties of the flood – high peak, short duration and the small changes along the course of the channel. The principal energy expenditure was on the entrainment and transport of boulders, both natural and concrete.

## 7. Acknowledgements

The authors wish to thank N. Yoselevich of the Cartography Laboratory, the Geography Department, University of Haifa for drawing the figures and The Royal Geographical Society Thesiger-Oman Fellowship 2016 to P.A. Carling.

## 8. References

Baker, V. R., 1987. Paleoflood hydrology and extraordinary flood events. Journal of Hydrology 96, 79-99. Doi: 10.1016/0022-1694(87)90145-4

Baker, V. R., 2003. A bright future for old flows: origins, status and future of paleoflood hydrology. In: Thorndycraft, V.R.G., Benito, G., Barriendos, M., Llassat, M.C., (Eds.), Paleofloods, Historical Data and Climatic Variabillity: Applications in Flood Risk Assessment. pp. 13-18.

Baker, V.R., Costa, J.E., 1987. Flood Power. In: Mayer, L., Nash, D., (Eds.), Catastrophic Flooding. Unwin, Boston and London, pp. 1-21.

Baker, V.R., Kochel, R.C., Patton, P.C., 1979. Long-term flood-frequency analysis using geological data. International Association Hydrological Science Publication 128, 3-9.

Baker, V.R., Ritter, D.F., 1977. Competence of rivers to transport coarse bed load material. Geological Society of America Bulletin 86, 975-978.

Baker, V.R., Kochel, R.C., 1988. Flood sedimentation in bedrock fluvial systems. In: Baker, V.R., Kochel, R.C., Patton, P.C., (Eds.), Flood Geomorphology. pp. 123-128, John Wiley & and Sons, New York.

Benito, G., Sanchez-Moya, Y.,Sopena, A., 2003. Sedimentology of high-stage flood deposits of the Tagus River, central Spain. Sedimentary Geology 157, 107-132. Doi: 10.1016/S0037-0738(02)00196-3

Benito, G., Lang, L., Barriendos, M., Llasat, M.C., Francies, F., Ouarda, T., Thorndycraft, V.R.G., Enzel, Y., Bardossy, A., Coeur, D., Bobee, B., 2004. Use of systematic, palaeoflood and historical data for the improvement of flood risk estimation. Review of scientific methods. Natural Hazards 31, 623-643.

Brunsden, D., Thornes, J. B, 1979. Landscape sensitivity and change. Transactions of the Institute of British Geographers NS 4, 463-84.

Carling. P.A, 1986. The Noon Hill flash floods; July 17th 1983. Hydrological and geomorphological aspects of a major formative event in an upland landscape Transactions of the Institute of British Geographers 11, 105-118.

Carling, P.A., (in press). Particle comminution defines megaflood energetics. Earth-Science Reviews.

Carling, P.A., Glaister, M.S, 1987. Reconstruction of a flood resulting from a moraine-dam failure using geomorphological evidence and dam-break modelling. 18th Annual Geomorphological Symposium, 'Catastrophic Flooding', Miami University, Ohio, 181-200.

Carling, P.A., Hoffmann, M., Blatter, A.S., 2002. Initial motion of boulders in bedrock channels. In: House, P.K., Webb, R.H., Baker, V.R., Levish, D.R., (Eds.), Ancient Floods, Modern Hazards: Principles and Applications of Paleoflood Hydrology. Water Science and Applications, 5, American Geophysical Union, pp. 147-160.

Carling, P.A., Tinkler, K.J., 1998. Conditions for entrainment of cuboid boulders in bedrock streams: an historical review of literature with respect to recent investigations. In: Tinkler, K.J., Wohl, E.E., (Eds.), Rivers over Rock: Fluvial Processes in bedrock Channels. American Geophysical Union, pp. 19-34.

Chorley, R. J., Morgan, M. A., 1962. Comparison of morphometric features, Unaka Mountains, Tennessee and North Carolina, and Dartmoor, England. Geological Society of America Bulletin 73, 17-34.

Costa, J., 1983. Paleohydraulic reconstruction of flash flood peaks from boulder deposits in the Colorado Front Range. Geological Society of America Bulletin 94, 986-1004.

Costa, J.E., O'Connor, J.E., 1995. Geomorphic effective floods. In: Costa, J.E., Miller, A.J., Potter, K.W., Wilcock, P.R., (Eds.), Natural and Anthropogenic Influences in Fluvial Geomorphology. American Geophysical Union, Geophysical Monograph 89, pp. 45-56.

Dayan, U., Ziv, B., Margalit, A., Morin, E., Sharon, D., 2001. Severe autumn storm over the Middle-East: Synoptic and mesoscale convection analysis. Theoretical and Applied Climatology 69, 103– 122. Doi: 10.1007/s007040170

Dayan, U., Morin, E., 2006. Flash floods-producing rainstorms over the Dead Sea: A review. In: Enzel, Y., Agnon, A., Stein, M., (Eds.), New Frontiers in Dead Sea Paleoenvironment Research. Geological Society of America Special Paper 401, pp 53-62.

Ely, L. L., Baker, V.R., 1985. Reconstructing paleoflood hydrology with slackwater deposits, Verde River, Arizona. Physical Geography 6, 103-126. Doi: 10.1080/02723646.1985.10642266

England Jr, J.F. et al., 2019. Guidelines for determining flood flow frequency—Bulletin 17C. 4-B5, Reston, VA.

Faershtein G., Porat N., Avni Y., Matmon A. (2016). Aggradation-incision transition in arid environments at the end of the Pleistocene: an example from the Negev Highlands, southern Israel. Geomorphology 253, 289-304. Doi: 10.1016/j.geomorph.2015.10.017

Frances, F., 2004. Flood frequency analysis using systematic and non-systematic information. In: Benito, G., Thorndycraft, V.R.G., (Eds.), Systematic, Palaeoflood and Historical data for improvement of flood risk estimation. pp. 55-70, The SPHERE project, CSIC, Madrid, Spain.

Fruchter, N., Matmon, A., Avni, Y., Fink, D., 2011. Revealing sediment sources, mixing, and transport during erosional crater evolution in the hyper-arid Negev Desert, Israel. Geomorphology 134 (3-4), 363–377. Doi: 10.1016/j.geomorph.2011.07.011

Garti, R., Moshe, I., Getker, M., Arbel, S., Lazanov, M., Zaguri, S., 1994. Floods generated during the 21–22 December 1993 rainstorm in the northern, central and southern Negev, Israel. Soil Erosion Research Station (SERS), Special Publication Report M-47. Ministry of Agriculture, Jerusalem. State of Israel, 48 pp (in Hebrew).

Garti, R., Arbel, S., Getker, M., 1998. High magnitude floods that occurred at the Negev and Arava drainage basins during the hydrological year 1997/98. Soil Erosion Research Station (SERS) Special Publication Report M-60. Ministry of Agriculture, State of Israel (in Hebrew).

Getker, M., Arazi, A., 2006. Extreme rainfall event at the Dead Sea region on the 29.10.2004. Soil Erosion Research Station, Ministry of Agriculture, State of Israel, 28 pp (in Hebrew).

Graham, J.R., 1998. Erosion of Concrete in Hydraulic Structures Reported by ACI Committee 210. Report ACI 210R-93, 24pp.

Greenbaum, N., 1996. Paleofloods in the large ephemeral stream systems of the central Negev. Ph.D. dissertation, Hebrew University of Jerusalem, 163 pp. (in Hebrew with English abstract).

Greenbaum, N., 2007. Assessment of dam-failure flood and a natural, high-magnitude flood in a hyperarid region using paleoflood hydrology, Nahal Ashalim catchment, Dead Sea, Israel. Water Resources Research 43, W02401, Doi: 10.1029/2006wr004956, 17P.

Greenbaum, N., Margalit, A., Schick, A.P., Sharon, D., Baker, V.R., 1998. A high magnitude storm and flood in a hyperarid catchment, Nahal Zin, Negev desert, Israel. Hydrological Processes 12, 1-23. Doi: 10/1002/(SICI)1099-1085(199801)12:1

Greenbaum, N., Schick, A.P., Baker, V.R., 2000. The paleoflood record of a hyperarid catchment, Nahal Zin, Negev Desert, Israel. Earth Surface Processes and Landforms 25, 951-971. Doi: 10/1002/1096-9837(200008)25:9

Greenbaum, N., Enzel, Y., Schick, A.P., 2001. Magnitude and frequency of paleofloods and historical floods in the Arava basin, Negev Desert, Israel. Israel Journal of Earth Sciences 50, 159-186.

Greenbaum, N., Schwartz, U., 2005. The 29.10.2004 rainstorm and floods in the northeastern Negev and the Dead Sea area. Dead Sea Works Ltd. Report, Beer-Sheva, Israel. 22p.

Greenbaum, N., Ben-Zvi, A., Haviv, I., Enzel, Y., 2006. The hydrology and paleohydrology of the Dead Sea tributaries. In: Enzel, Y., Agnon, A., Stein, M., (Eds.), New Frontiers in Dead Sea Paleoenvironment Research. Geological Society of America Special Paper 401, pp. 63-93. Doi: 10.1130/2006.2401(05)

Greenbaum, N., Lekach, J., 1997. The potential water resource and efficiency of detention storage of the reservoirs in the Makhtesh Katan catchment. Report to Mekorot Water Company Ltd., Hebrew University Jerusalem, 26 pp. (in Hebrew).

Greenbaum, N., Schwartz, U., Bergman, N., 2010. Extreme floods and short-term hydroclimatological fluctuations in the hyper-arid Dead Sea region, Israel. Global and Planetary Change 70, 125-137. Doi:10.1016/j.gloplacha.2009.11.013.

Greenbaum, N., Wittenberg, L., Schwartz, U. (2009). Boulders transport during the extreme October 2004 flood in Nahal Hatzera. Field excursion guidebook, GLOCOPH Israel conference, October 2009, p.197.

Greenbaum, N., Harden, T.M., Baker, V.R., Weisheit, J., Cline, M.L., Porat, N., Halevi, R., Dohrenwend, J., 2014. A 2000 year natural record of magnitudes and frequencies for the largest Upper Colorado River floods near Moab, Utah. Water Resources Research. Doi: 10.1002/2013WR014835.

Hydrologic Engineering Center, 2018. HEC-RAS: Water River Analysis System, Version 5.0.5, U.S. Army Corp. of Eng., Davis, California.

Inbar, M., 2000. Episodes of Flash Floods and Boulder Transport in the Upper Jordan River. IAHS Publication 261. IAHS Press: Wallingford, UK. pp. 185–200.

Kahana, R., Ziv, B., Enzel, Y., Dayan, U., 2002. Synoptic climatology of major floods in the Negev desert, Israel. International Journal of Climatology 22, 867-882. Doi: 10.1002/joc.766

Kale, V.S., 2007. Geomorphic effectiveness of extraordinary floods on three large rivers of the Indian Peninsula. Geomorphology 85, 306–316. Doi: 10.1016/j.geomorph.2006.03.026

Kale, V.S., Hire, P.S., 2004. Effectiveness of monsoon floods on the Tapi River, India: role of channel geometry and hydrologic regime. Geomorphology 57, 275–291. Doi: 10.1016/S0169-555X(03)00107-7

Klemeš, V., 2000. Tall Tales about Tails of Hydrological Distributions. #x2003; I. Journal of Hydrologic Engineering 5(3), 227-231

Kochel, R. C., Baker, V.R., 1982. Paleoflood hydrology. Science 215, 353-361. Doi: 10.1126/science.215.4531

Kochel, R. C., Baker, V.R., Patton, P. C., 1982. Paleohydrology of southwestern Texas. Water Resources Research 18, 1165-1183.

Komar, P.D., 1987. Selective gravel entrainment and the empirical evaluation of flow competence. Sedimentology 34, 1165-1176. Doi: 10.1111/j.1365-3091.1987.tb0059

Lamb, M.P., Finnegan, N.J., Scheingross, J.S., Sklar, L.S., 2015. New insights into the mechanics of fluvial bedrock erosion through flume experiments and theory. Geomorphology 244, 33-55. Doi: 10.1016/j.geomorph.2015.03.003

Lisenby, P.E., Croke, J., Fryirs, K.A., 2018. Geomorphic effectiveness: a linear concept in a non-linear world. Earth Surface Processes and Landform 43, 4-20. Doi: 10.1002/esp.4096

National_Research_Council, 1988. Estimating Probabilities of Extreme Floods: Methods and Recommended Research. The National Academies Press, Washington, DC, 160 pp.

O'Connor, J. E., 1993. Hydrology, hydraulics and geomorphology of the Bonneville flood. Geological Society of America Special Paper 274, 83 p.

O'Connor, J. E., Webb, R.H., 1988. Hydraulic modelling for paleoflood analysis. In: Baker, V.R., Kochel, R.C., Patton, P.C., (Eds.), Flood Geomorphology. pp. 383-402, John Wiley & and Sons, New York.

O'Connor, J.E., Ely, L.L., Wohl, E., Stevens, L.E., Melis, T.S., Kale, V.S., Baker, V.R., 1994. A 4500-year record of large floods on the Colorado River in the Grand Canyon, Arizona. Journal of Geology 102, 1-9. Doi: 10.1086/629644

O'Connor, J. E., Baker, V.R., Webb, R.H., 1986. Paleohydrology of pool and riffle pattern development, Boulder Creek, Utah. Geological Society of America Bulletin 97, 410– 420. Doi: 10/1130/0016-7606(1986)97

Partridge, J. B., Baker, V.R., 1987. Paleoflood hydrology of the Salt River, central Arizona. Earth Surface Processes and Landforms 12, 109-125. Doi: 10.1002/esp.3290120202

Patton, P. C., Baker, V.R., Kochel, R.C. 1979. Slack-water deposits: a geomorphic technique for the interpretation of fluvial paleohydrology. In: Rhodes, D.D., Williams, G.P., (Eds.), Adjustment of the Fluvial System, pp. 225-253, Kendall/Hunt, Dubuque, Iowa.

Plakht, J., 2003. Quaternary maps of Makhtesh Hatira and Makhtesh Hazera, Negev Desert. Israel Journal of Earth Science 52, 31-38.

Polak, S., 1988. Maximal peak discharges after the rainstorm of the 17–18.10.1987 Report Hydro/2/1988, Israel Hydrological Service, Jerusalem, 23 pp (in Hebrew).

Porat, N., Rosen, S.A., Avni, Y., Boaretto, E., 2006. Dating the Ramat Saharonim Late Neolithic Deser Cult site. Journal of Archaeological Sciences 33, 1341-1355. Doi: 10/1016/j.jas.2006.01.008

Schumm, S. A., 1973. Geomorphic thresholds and complex response of drainage system', in M. Morisawa (ed.) Fluvial Geomorphology, Proc. 4th Annual Geo-morph. Symp. (Binghampton, N.Y.), 299-310.

Stedinger, J. R., Cohn, T.A., 1986. Flood frequency analysis with historical and paleoflood information. Water Resources Research 22, 785-793. Doi: 10.1029/WR022i005p00785

Stedinger, J., Therivel, R., Baker, V.R., 1988. Flood frequency analysis with historical and paleoflood information, Salt and Verde Rivers, Arizona. In: Proceedings of the Eighth Annual Meeting of the U.S. Committee on Large Dams, Salt River Project, Phoenix, Arizona, 3.1-3.35.

Survey of Palestine, 1946. Prepared in 1945-1946 for the information of the Anglo-American Committee of Inquiry, by the British Government in Palestine.

Tasker, G.D., Stedinger, J.R., 1989. An operational GLS model for hydrologic regression. Journal of Hydrology 111(1), 361-375. Doi: 10.1016/0022-1694(89)90268-0

Thorndycraft, V. R., Benito, G., Llasat, N.C., Barriendos, M., 2003. (Eds.), Paleofloods, Historical Data and Climatic Variability: Applications in Flood Risk Assessment, Proceedings of the PHEFRA International workshop, October 2002, Barcelona, Spain, 378 pp.

van Rijn, L.C., 2019. Critical movement of large rocks in currents and waves. International Journal of Sediment Research 34, 387-398.

Webb, R. H., O'Connor, J.E., Baker, V.R., 1988. Paleohydrologic reconstruction of flood frequency on the Escalante River, south central Utah. In: Baker, V.R., Kochel, R.C., Patton, P.C., (Eds.) Flood Geomorphology. pp. 403-418, John Wiley & and Sons, New York.

Webb, R.H., Jarrett, R.D., 2002. One-dimensional estimation techniques for discharges of paleofloods and historical floods. In: House, P.K., Baker, V.R., Webb, R.H., Levish, D.H., (Eds.), Ancient Floods, Modern Hazards: Principles and Applications of Paleoflood Hydrology. Water Science Applications, Series 5, pp. 111-126, AGU, Washington, D.C.

Williams, G.P., 1983. Paleohydrological methods and some examples from Swedish fluvial environments, I.-Cobble and boulder deposits. Geografiska Analar 65A, 227-243. Doi: 10.1080/04353676.1983.11880088

Wohl, E.E., 1998. Uncertainty in flood estimates associated with roughness coefficient. Journal of Hydraulic Engineering 124, 291-223.

Wolman, M.G., Gerson, R., 1978. Relative scales of time and effectiveness of climate in watershed geomorphology. Earth Surface Processes 3, 189-208. Doi: 10.1002/esp.3290030207

Wollman, M.G., Miller, J.P., 1960. Magnitude and frequency of forces in geomorphic processes. Journal of Geology 68, 54-74. Doi:10.2307/30058255

Zilberman, E., 2000. Formation of "Makhteshim" – unique erosion cirques in the Negev, southern Israel. Israel Journal 0f Earth Science 49, 127-141.

Ziv, B., Dayan, U., Sharon, D., 2004. A mid-winter, tropical extreme flood-producing storm in southern Israel: synoptic scale analysis. Meteorology and Atmospheric Physics. Doi:10.1007/s00703-003-0054-7.



**Figure Captions**

Figure 1: The study area of the major drainage system of Nahal Zin in the northeastern Negev, including rainfall amounts and peak discharges of the various tributaries during the October 2004 rainstorm, the study basin of Nahal Hatzera and the study site at the outlet of the Makhtesh Hatzera Erosion Cirque (MHEC). Data derived from: IHS – Israel Hydrological Service; SERS – Soil Erosion Research Station; IMS – Israel Meteorological Service.

Figure 2: The drainage basin of Nahal Hatzera and the borders of the Makhtesh Hatzera Erosion Cirque (MHEC; 45 $km^2$) - airphoto and figure. **(a)** Drainage area within the MHEC (30 $km^2$); **(b)** Drainage area outside the cirque (15 $km^2$). Note the opposite directions of the tributaries inside the MHEC (southeast) and outside the MHEC

(northwest) related to the reversal of the drainage system into the nearby Dead Sea Rift during the Plio-Pleistocene. The study site is located at the only outlet of the MHEC. Note the similar distances between the water divide and the outlet of the major tributaries and their confluence close to the outlet. The colored patches at the bottom are exposures of sandstone, the rest are gravelly Pleistocene and Holocene alluvial surfaces

Figure 3: Temporal distribution of rainfall during the 2004 rainstorm as measured at the rain-gage of Sedom (74 mm) and reconstructed for two locations within the MHEC using non-calibrated rainfall radar (60-70 mm) (Getker and Arazi, 2006). Note that the duration of the rainstorm at all stations was 1.5-2 hours generating extremely high 10-minutes intensities of up to 175 mm $hr^{-1}$.

Figure 4: Drone ortho-photo showing the 2 segments of the 500 m long study reach, the SWD stratigraphic sections (MK1-MK4, figure 6), the boulder bar (Figure b), cross section 17 (Figure 8), and the electricity pole (Figures 5a and 7b). A car encircled in red for scale.

Figure 5: (a) The electricity pole at the inlet constriction to the gorge with a person for scale. Note the driftwood accumulated on the pole indicating water surface elevation of >8.5 m and the concrete channel which serves as a road. For location along the channel see also figures 5e and 7b. (b) the boulder bar at the upper segment of the study reach with concrete boulders B4, B6, B8 marked with arrows (see also figure 7b). Location of boulder B6 is shown in figures 5c and 8. (c) Boulder B6 - intermediate axis - 0.85 m, weight – 0.82 ton perched on natural boulder cluster. (d) Boulder B4 - intermediate axis – 1.05 m, weight – 1.56 tonnes, located at a low part of the boulder bar, flipped over and

imbricated against natural boulders. For location see figures 5b and 6. (e) The natural bedrock channel of the gorge after the 1994 flood (230 $m^3$ $s^{-1}$; Greenbaum and Lekach, 1997) which completely evacuated the British road. The residual concrete anchor of the road is located along the left bank of the gorge. The pipe transported water from a well within the MHEC to factories outside. The electricity pole is marked in black arrow (see also figures 4, 5a and 7b). View is looking upstream.

Figure 6: Stratigraphy and chronology of the four SWD paleoflood sections along the study site: (a) MK1 (b) MK2 (c) MK3 (d) MK4. Each section contains 3-8 sedimentary units composed mostly of coarse-fine sand. Note that the OSL ages ka BP (2018) are much older than the radiocarbon ages AD. MK4 is located within a cave at the outlet of the gorge (Greenbaum, 1996). For locations of the sections see figure 4.

Figure 7: Water surface profiles (WSPs) along the study reach at the outlet of the MHEC using HEC-EAS hydraulic program. (a) in relation to the paleoflood stratigraphic sections (MK1-MK4) and in relation to the reconstructed natural bedrock channel (see figure 5e). Note the two hydraulic jumps and associated backwaters related to the abrupt channel constrictions (b) in relation to the high water marks (HWM) of the 2004 flood assigning a peak discharge of about 470 $m^3$ $s^{-1}$ to the flood. The channel is the concrete channel bed. Note the depositional locations of the concrete boulders (in red squares) (see figures 5c and 5d) related to the hydraulic jump. The electricity pole at the inlet to the gorge is shown in figures 4, 5a and 5e.

Figure 8: Cross-section 17 at the upper segment of the study reach including the water surface elevation of the 2004 flood. For location see figure 4. Boulder B7 (intermediate

axis – 1.5 m; weight – 4.92 tonnes) is located in the channel bed, whereas boulder B6 (intermediate axis - 0.85 m; weight – 0.82 tonne) was deposited over the large boulder bar on the right bank at the middle of the section. Boulder 6 is shown in figures 5b and 5c.

Figure 9: Flood frequency analysis using MAX program (Stedinger et al. 1988) for four distributions. The best fit to the paleoflood data (black circles) was obtained for the Pearson III distribution, which assigned the 2004 flood a recurrence interval of about 120 years.

Figure 10: Relation between boulder size and the calculated shear stress for boulder transport in Nahal Hatzera (gray symbols) compared to the results of Greenbaum et al. (2009) and other studies (modified from O'Connor, 1993).

**Table 1: Historical and paleoflood data for the Nahal Hatzera ephemeral stream**

| No. of floods | Peak discharge ($m^3 s^{-1}$) | OSL Age<br>Ka before 2018 | Radiocarbon Age<br>Calibrated years AD | Location of evidence | Source of data |
|---|---|---|---|---|---|
| 1 | 760 | | | SWD Rt. bank | Present study |
| 6<br>5<br>4<br>3<br>2<br>1 | 550<br>500<br>475<br>450<br>440<br>400 | 8.0±0.7 ka<br><br>12.0±0.7 ka<br><br>13.9±1.4 ka | 1489-1644 AD | MK-1 - Overbank deposit at the inlet to the gorge – Lt. bank | Present study |
| 5<br>4<br>3<br>2<br>1 | 290<br>265<br>245<br>230<br>200 | 4.5±0.4 ka | 1445-1634 AD | MK-2 – Rock shelter at the inlet to the gorge – Lt. bank | Present study |
| 3<br>2<br>1 | 430<br>400<br>380 | 4.8±0.6 ka | 1689-1926 AD | MK-3 - Section in the Gorge – Rt. bank | Present study |
| 8 | 250-300 | Unit 1 – 10.5±0.8 ka<br>Unit 7 – 7.8±0.7 ka | | MK-4 - Gorge Cave – Lt. bank | Greenbaum (1996) |
| 1 | 230 | 1994 AD | Observed flood | Driftwood and erosion lines | Greenbaum & Lekach (1997) |
| 1 | 470<br>600<br>580 | 2004 AD | Observed flood | Driftwood line along the entire study reach | Present study<br>Greenbaum & Schwartz (2005)<br>Arbel et al. (2007);<br>Greenbaum et al. (2009; 2010) |
| 1 | 130 | 2018 AD | Observed flood | Driftwood line | Present study |

**Table 2: Nahal Hatzera boulder data**

| Long axis (L) (m) | Intermediate Axis (M) (m) | Short axis (S) (m) | Cubed root 3√(L*M*S) (m) | Equivalent Cuboid Volume L*M*S ($m^3$) | Equivalent Ellipsoid Volume 4/3*22/7* L/2*M/2*S/2 ($m^3$) |
|---|---|---|---|---|---|
| **Immobile natural blocks** | | | | | |
| 5.0 | 4.0 | 3.7 | 4.2 | 74.0 | 38.76 |
| 8.3 | 3.3 | 1.8 | 3.67 | 49.3 | 25.82 |
| 4.7 | 4.1 | 2.3 | 3.54 | 44.32 | 23.22 |
| 3.8 | 3 | 2.6 | 3.09 | 29.64 | 15.53 |
| 3.8 | 3.4 | 2.0 | 2.96 | 25.84 | 13.54 |
| 4.2 | 3.0 | 1.6 | 2.72 | 20.16 | 10.56 |
| 3.1 | 2.5 | 2.4 | 2.65 | 18.6 | 9.74 |
| 3.5 | 3.0 | 1.6 | 2.56 | 16.8 | 8.8 |
| 4.0 | 2.8 | 1.4 | 2.5 | 15.68 | 8.21 |
| **4.49** | **3.23** | **2.16** | **3.10** | **32.7** | **17.13** |
| *1.54* | *0.53* | *0.71* | *0.58* | *19.59* | *10.57* |
| **Concrete blocks and slabs (the largest)** | | | | | |
| 1.7 | 0.85 | 0.3 | 0.76 | 0.43 | 0.23 |
| 2.9 | 1.3 | 0.85 | 1.47 | 3.2 | 1.68 |
| 1.35 | 0.85 | 0.3 | 0.7 | 0.34 | 0.18 |
| 2.1 | 1.5 | 0.65 | 1.27 | 2.05 | 1.07 |
| 2.6 | 1.6 | 0.7 | 1.43 | 2.91 | 1.53 |
| 2.05 | 1.05 | 0.3 | 0.86 | 0.65 | 0.34 |
| 3.4 | 1.45 | 1.3 | 1.80 | 6.41 | 3.36 |
| 3.6 | 1.2 | 0.9 | 1.57 | 3.89 | 2.04 |
| **2.46** | **1.23** | **0.66** | **1.24** | **2.49** | **1.3** |
| *0.86* | *0.29* | *0.38* | *0.44* | *2.25* | |
| **Mobile natural boulders** | | | | | |
| 25 | 2.1 | 1.0 | 1.74 | 5.25 | 2.75 |
| 1.8 | 1.8 | 1.6 | 1.73 | 5.18 | 2.72 |
| 1.9 | 1.4 | 1.3 | 1.51 | 3.46 | 1.81 |
| 3.0 | 1.3 | 0.7 | 1.4 | 2.73 | 1.43 |
| 2.0 | 1.3 | 0.7 | 1.22 | 1.82 | 0.95 |
| 1.4 | 1.4 | 0.4 | 0.92 | 0.78 | 0.41 |
| 1.45 | 0.6 | 0.57 | 0.79 | 0.5 | 0.26 |
| 0.9 | 0.88 | 0.33 | 0.64 | 0.26 | 0.14 |
| **1.87** | **1.35** | **0.83** | **1.24** | **2.5** | **1.31** |
| *0.66* | *0.47* | *0.44* | *0.42* | *2.01* | |
| **Possibly mobile natural blocks and boulders** | | | | | |
| 2.8 | 2.3 | 1.3 | 2.03 | 8.37 | 4.39 |
| 2.4 | 1.6 | 1.4 | 1.75 | 5.38 | 2.82 |
| 1.7 | 1.7 | 1.4 | 1.59 | 4.05 | 2.12 |
| 2.8 | 1.8 | 0.7 | 1.52 | 3.53 | 1.85 |
| 2.2 | 1.2 | 0.9 | 1.33 | 2.38 | 1.24 |
| 2.2 | 1.4 | 0.7 | 1.29 | 2.16 | 1.13 |
| **2.35** | **1.67** | **1.07** | **1.59** | **4.31** | **2.26** |
| *0.42* | *0.38* | *0.34* | *0.28* | *2.31* | |

**Bold -** average; *Italic* – Standard deviation

**Table 3: Makhtesh Hatzera OSL ages**

| Description | Depth (m) | Water contents (% est.) | Dose rate (µGy/a) | No. aliquots | OD (%) | De (Gy) | Age (ka) | FMM De (Gy) | Model ages (ka) | |
|---|---|---|---|---|---|---|---|---|---|---|
| | | | | | | | | | FMM age | MA |
| MK1 - SWD, unit 2 | 2.3 | 2 | 696±26 | 43/50 | 78 | 25±12 | 36±18 | 9.7±0.9 | **13.9±1.4** | |
| MK1 – SWD, unit 4 | 1.05 | 2 | 870±31 | 57 | 87 | 24±20 | 27±23 | 10.4±0.4 | **12.0±0.7** | |
| MK1 – SWD, unit 6 | 0.35 | 2 | 841±29 | 46/56 | 90 | 20±12 | 24±14 | 6.8±0.6 | **8.0±0.7** | |
| MK2 - SWD, unit 5 | 3 | 2 | 746±23 | 55/65 | 88 | 17±11 | 35±15 | 3.3±0.3 | **4.5±0.4** | |
| MK4 – cave, SWD, unit 7 | 0.07 | 2 | 788±25 | 29/42 | 69 | 16±6 | 21±8 | 9.5±0.4 | **12.0±0.6** | **7.** |
| MK4 – cave, SWD, unit 2 | 0.62 | 2 | 800±24 | 35/42 | 70 | 21±10 | 26±12 | 14.4±0.3 | **18.0±0.7** | **10** |
| MK3 – SWD, unit 2 | 0.52 | 2 | 979±29 | 31/41 | 90 | 26±13 | 26±14 | 6.9±0.3 | **7.0±0.4** | **4.** |

Methods:

88-125 µm quartz was purified by wet-sieving to the selected grain size, dissolving carbonates by 8% HCl, removing heavy minerals and most feldspars by magnetic separation, and dissolving the remaining feldspars and etching the quartz with 40% HF (for 40 min), followed by soaking in 16% HCl overnight to dissolve any fluorides which may have precipitated.

Samples were measured using a preheat of 10s @ 260°C, a test dose of ~4.6 Gy and a test dose preheat of 5 s @ 200 °C. De was measured on 1 mm aliquots using a modified single aliquot regenerative (SAR) protocol. All samples show recycling ratios within 8% of 1.0 for most aliquots and negligible IR depletion ratios.

The average De and errors were calculated using unweighted mean. For samples for which more than 40 aliquots were measured, De valuse were also calculated using the Finite Mixture Model, which isolates different De components in the data.

Alpha, beta and gamma dose rates were calculated from the radioactive elements measured by ICP MS (U&Th) or ICP-OES (K). Cosmic dose rates were estimated from the current burial depths.

OD – Overdispersion. Aliquots used – the number of aliquots used for the average De out of the aliquots measured. Youngest age was calculated from N youngest aliquots.

**Table 4: Radiocarbon ages**

| Sample no. | Section and Sedimentary unit | Material | $^{14}$C Age<br>Years BP | Age<br>Cal. Years AD | 95.4% probability<br>Cal. Years AD |
|---|---|---|---|---|---|
| AA111242 | MK2, unit 4 | charcoal | 374 ± 32 | 1445-1634 | 1445-1528 (56.4%)<br>1552-1634 (39.0%) |
| AA112568 | MK1, unit 6 | wood | 319 ± 24 | 1489-1644 | 1489-1604 (74.7%)<br>1610-1644 (20.7%) |
| AA111243 | MK3, unit 2 | wood | 102 ± 22 | 1689-1926 | 1689-1730(26.1%)<br>1809-1926 (69.3%) |

**Table 5: Concrete boulders geometry and depositional hydraulic data**

| Boulder no. | Cross section no. | Intermediate axis (m) | Equivalent cuboid volume ($m^3$) | Weight* (tonne) | Water depth (m) | Froude No. | Velocity ($m\ s^{-1}$) | Shear Stress $N\ m^{-2}$ | Stream Power $N\ m^{-1}\ s^{-1}$ |
|---|---|---|---|---|---|---|---|---|---|
| 8 | 16 | 0.85 | 0.43 | 1.03 | 3.43 | 0.26 | 1.5 | 9.2 | 14 |
| 9 | 16 | 1.3 | 3.2 | 7.68 | 2.92 | 0.28 | 1.5 | 9.2 | 14 |
| 6 | 17 | 0.85 | 0.34 | 0.82 | 2.4 | 0.39 | 1.9 | 14.4 | 27 |
| 7 | 17 | 1.5 | 2.05 | 4.92 | 5.4 | 0.26 | 1.9 | 14.4 | 27 |
| 7A | 17 | 1.6 | 2.91 | 6.98 | 2.16 | 0.41 | 1.9 | 14.4 | 27 |
| 4 | 18 | 1.05 | 0.65 | 1.56 | 0.7 | 0.80 | 2.1 | 18.8 | 40 |
| 2 | 19 | 1.45 | 6.41 | 15.38 | 3.65 | 1.54 | 9.2 | 437.0 | 4020 |
| 1 | 21 | 1.2 | 3.89 | 9.34 | 1.64 | 1.99 | 8.0 | 300.0 | 2393 |

- Concrete specific weight – 2.4 ton $m^{-3}$
- Boulders locations are shown on figure 7b

**Table 6: Peak discharges ($m^3 s^{-1}$) for various return periods of the paleoflood record using MAX program** (Stedinger et al., 1988)

| Annual Exceedance Probability (%) | Average Recurrence Interval (years) | Log Pearson III | Log Normal | Normal | Pearson III |
|---|---|---|---|---|---|
| 10 | 10 | 177 | 150 | 20 | 80 |
| 5 | 20 | 235 | 220 | 170 | 198 |
| 2 | 50 | 340 | 340 | 342 | 345 |
| 1 | 100 | 452 | 453 | 455 | 453 |
| 0.5 | 200 | 597 | 590 | 559 | 560 |
| 0.2 | 500 | 867 | 813 | 685 | 694 |
| 0.1 | 1000 | 1120 | 1017 | 773 | 809 |

**Table 7: Maximum hydraulic values for various return periods along the upper segment, using Pearson 3 distribution**

| Return Period (years) | Discharge ($m^3$ $s^{-1}$) | Velocity (m $s^{-1}$) | Shear Stress (N $m^{-2}$) | Stream Power (N $m^{-1}s^{-1}$) |
|---|---|---|---|---|
| 10 | 80 | 7.1 | 350 | 2500 |
| 20 | 200 | 9.0 | 470 | 4222 |
| 50 | 350 | 9.8 | 507 | 4972 |
| 100 | 450 | 9.2 | 437 | 4020 |
| 200 | 560 | 8.9 | 420 | 3733 |
| 500 | 700 | 8 | 308 | 2500 |
| 1000 | 800 | 8 | 310 | 2523 |

**Declaration of interests**

☒ The authors declare that they have no known competing financial interests or personal relationships that could have appeared to influence the work reported in this paper.

☐The authors declare the following financial interests/personal relationships which may be considered as potential competing interests:

Noam Greenbaum

On behalf of all other authors

**Highlights**

- Large documented flood in ungauged basin, hyperarid region transported large concrete boulders that could be distinguished from natural boulders.
- Hydraulic analysis provide peak discharges and other values of all hydraulic parameters for each boulder
- Paleoflood hydrology documented 23 paleofloods during the last 600 years which enabled a flood frequency analysis (FFA)
- The results of the FFA provide return periods for peak discharges and the potential boulders transport

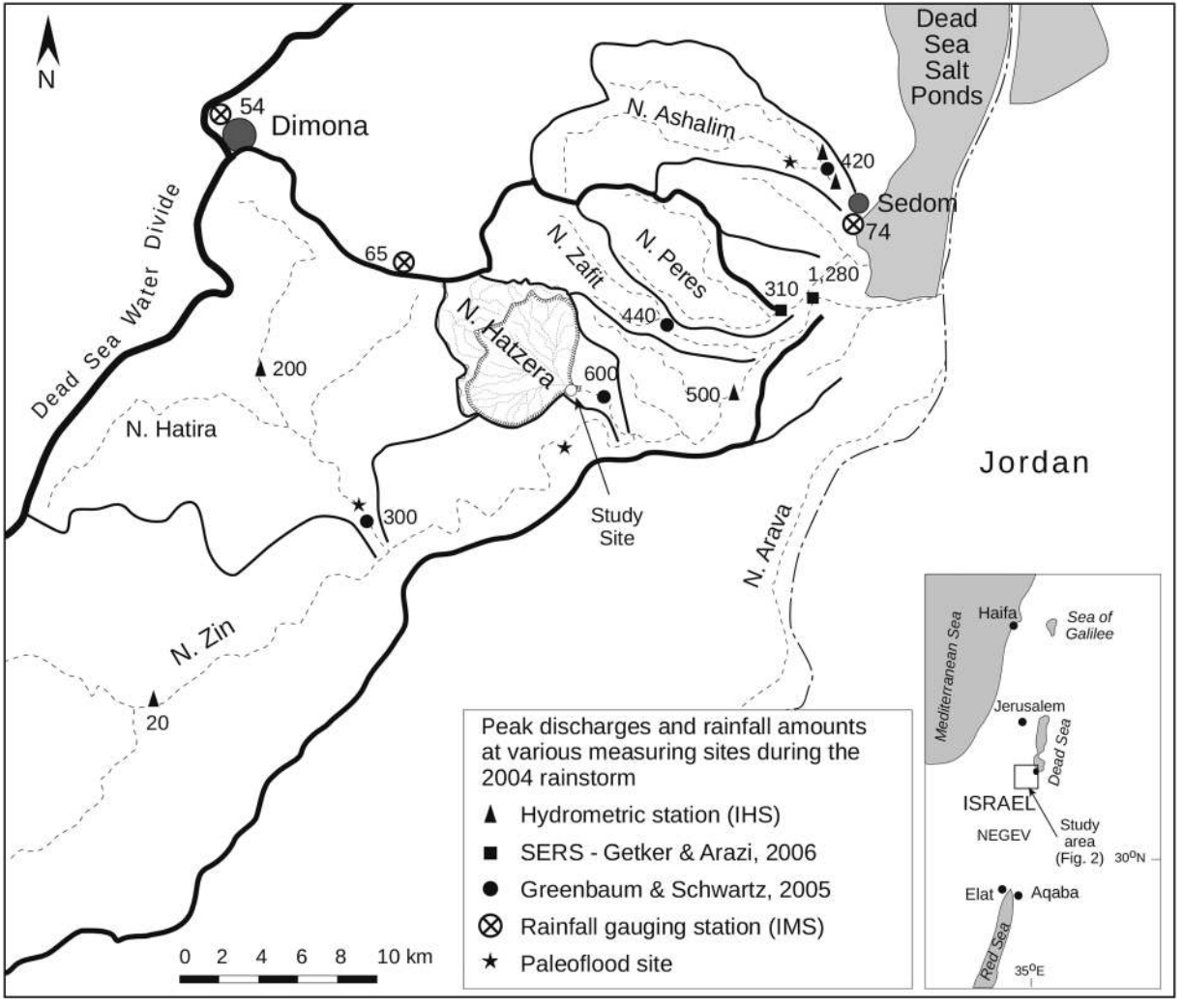
N
Dimona
54
Dead Sea Water Divide
65
N. Ashalim
420
Dead Sea Salt Ponds
Sedom
74
N. Zafit
N. Peres
310
1,280
440
N. Hatzera
600
500
200
N. Hatira
300
Study Site
N. Arava
Jordan
N. Zin
20
Peak discharges and rainfall amounts at various measuring sites during the 2004 rainstorm
Hydrometric station (IHS)
SERS - Getker & Arazi, 2006
Greenbaum & Schwartz, 2005
Rainfall gauging station (IMS)
Paleoflood site
0 2 4 6 8 10 km
Mediterranean Sea
Haifa
Sea of Galilee
Jerusalem
Dead Sea
ISRAEL
NEGEV
Study area (Fig. 2)
30°N
Elat
Aqaba
Red Sea
35°E

Figure 1


b
a
Nahal Hatzera
Erosion Cirque escarpment
Study site
0
1
2 km

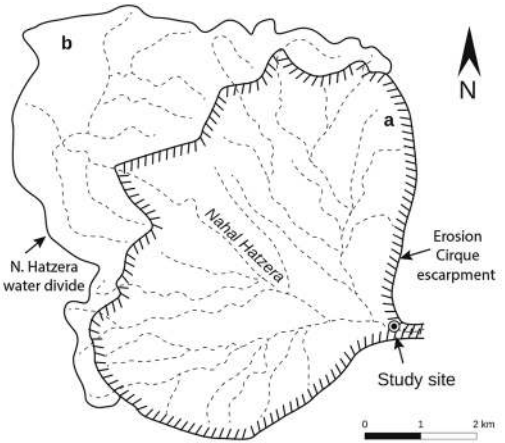
b
a
N
Nahal Hatzera
N. Hatzera water divide
Erosion Cirque escarpment
Study site
0
1
2 km

Figure 2

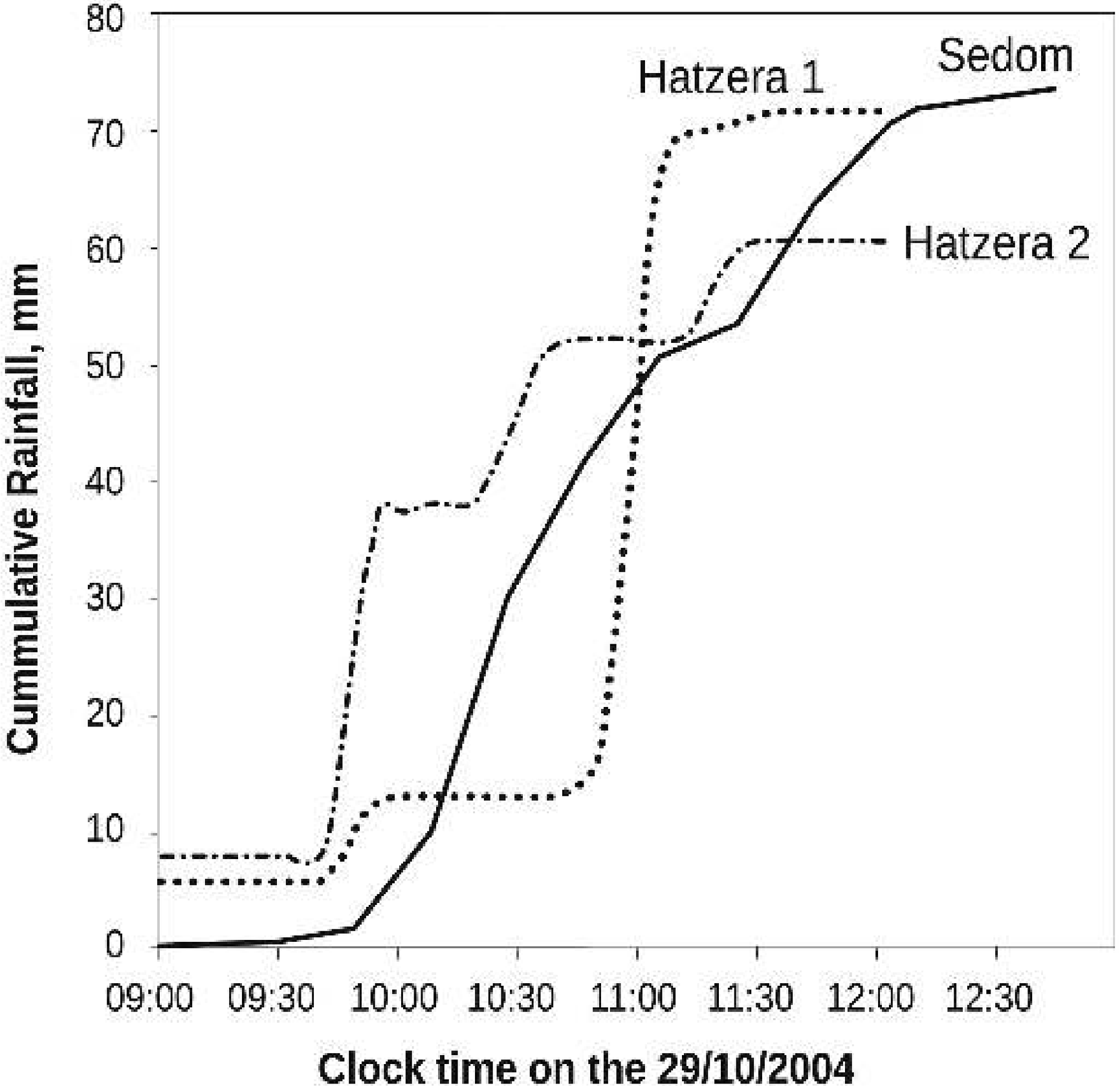
Sedom
Hatzera 1
Hatzera 2
Cummulative Rainfall, mm
0
10
20
30
40
50
60
70
80
09:00
09:30
10:00
10:30
11:00
11:30
12:00
12:30
Clock time on the 29/10/2004

Figure 3

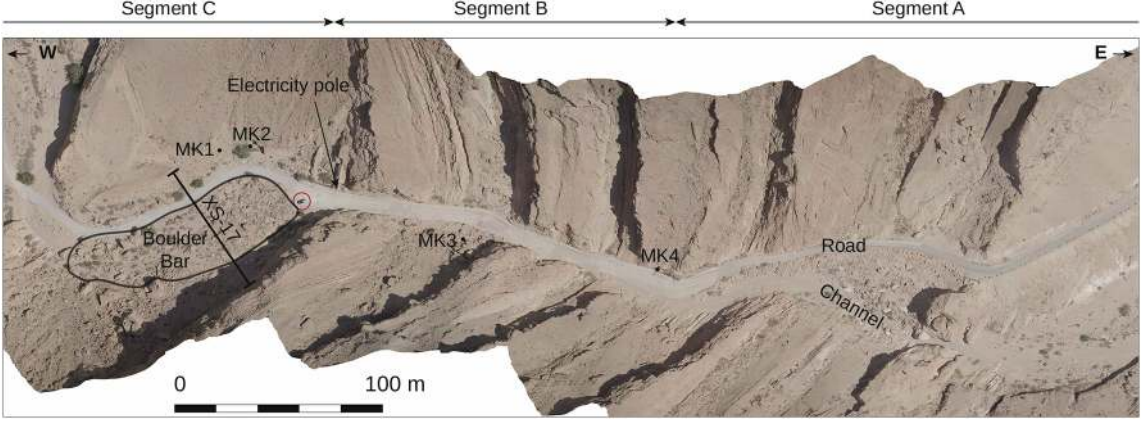
Segment C
Segment B
Segment A
W
E
Electricity pole
MK1
MK2
XS-17
Boulder Bar
MK3
MK4
Road
Channel
0
100 m

Figure 4

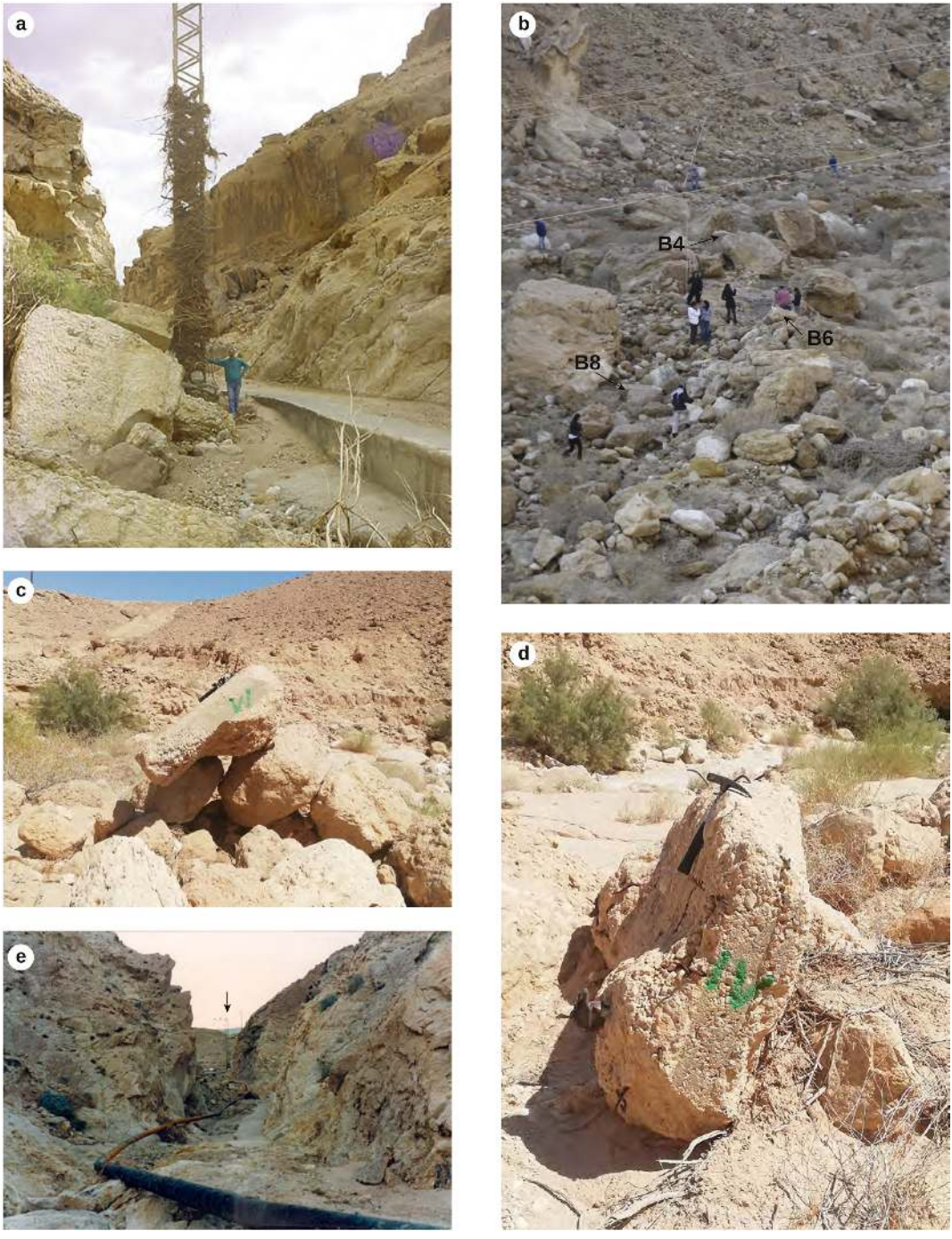


Figure 5

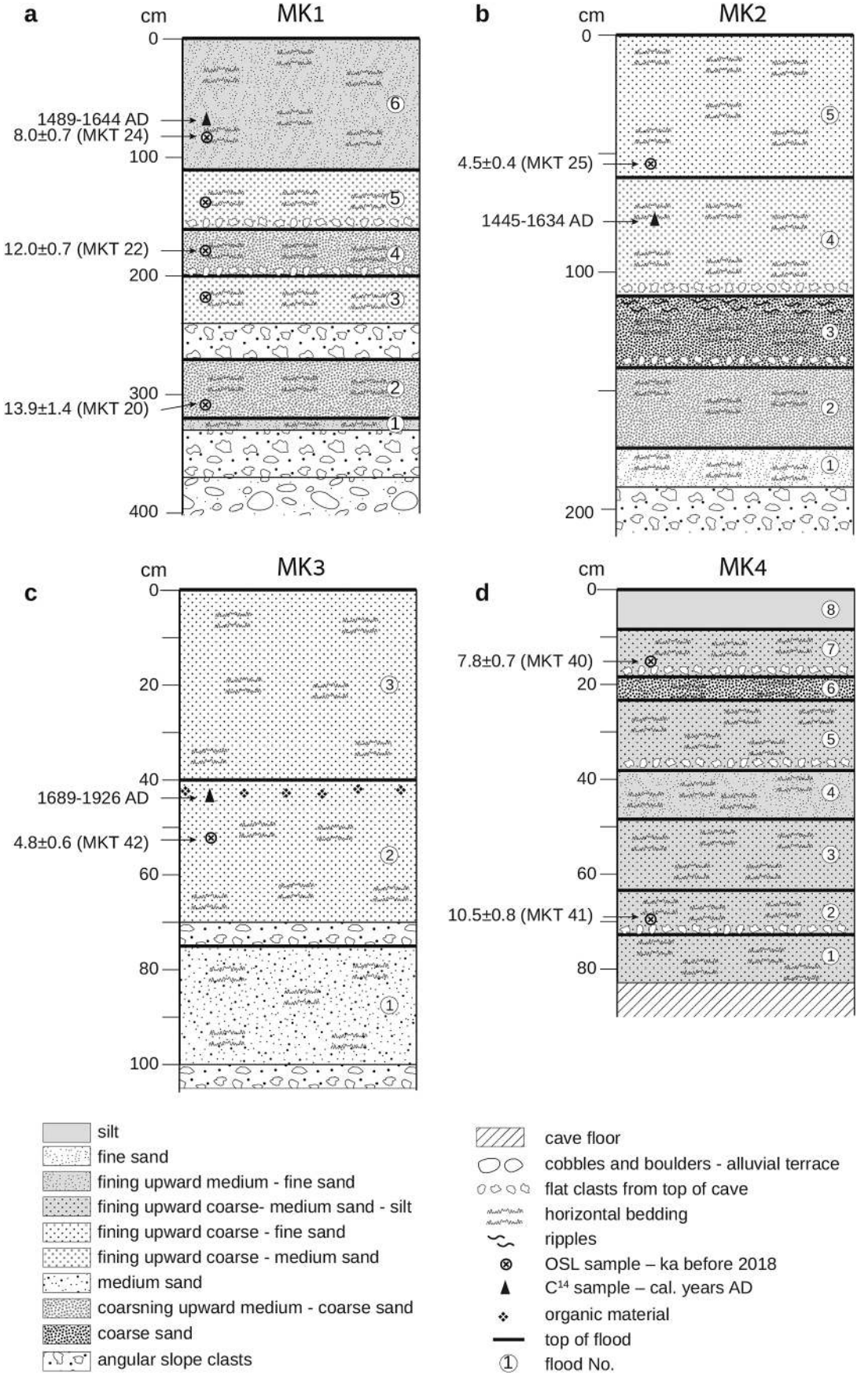
a
cm
MK1
0
1489-1644 AD
8.0±0.7 (MKT 24)
100
12.0±0.7 (MKT 22)
200
300
13.9±1.4 (MKT 20)
400
b
cm
MK2
0
4.5±0.4 (MKT 25)
1445-1634 AD
100
200
c
cm
MK3
0
20
40
1689-1926 AD
4.8±0.6 (MKT 42)
60
80
100
d
cm
MK4
0
7.8±0.7 (MKT 40)
20
40
60
10.5±0.8 (MKT 41)
80
silt
fine sand
fining upward medium - fine sand
fining upward coarse- medium sand - silt
fining upward coarse - fine sand
fining upward coarse - medium sand
medium sand
coarsning upward medium - coarse sand
coarse sand
angular slope clasts
cave floor
cobbles and boulders - alluvial terrace
flat clasts from top of cave
horizontal bedding
ripples
OSL sample – ka before 2018
C14 sample – cal. years AD
organic material
top of flood
flood No.

Figure 6

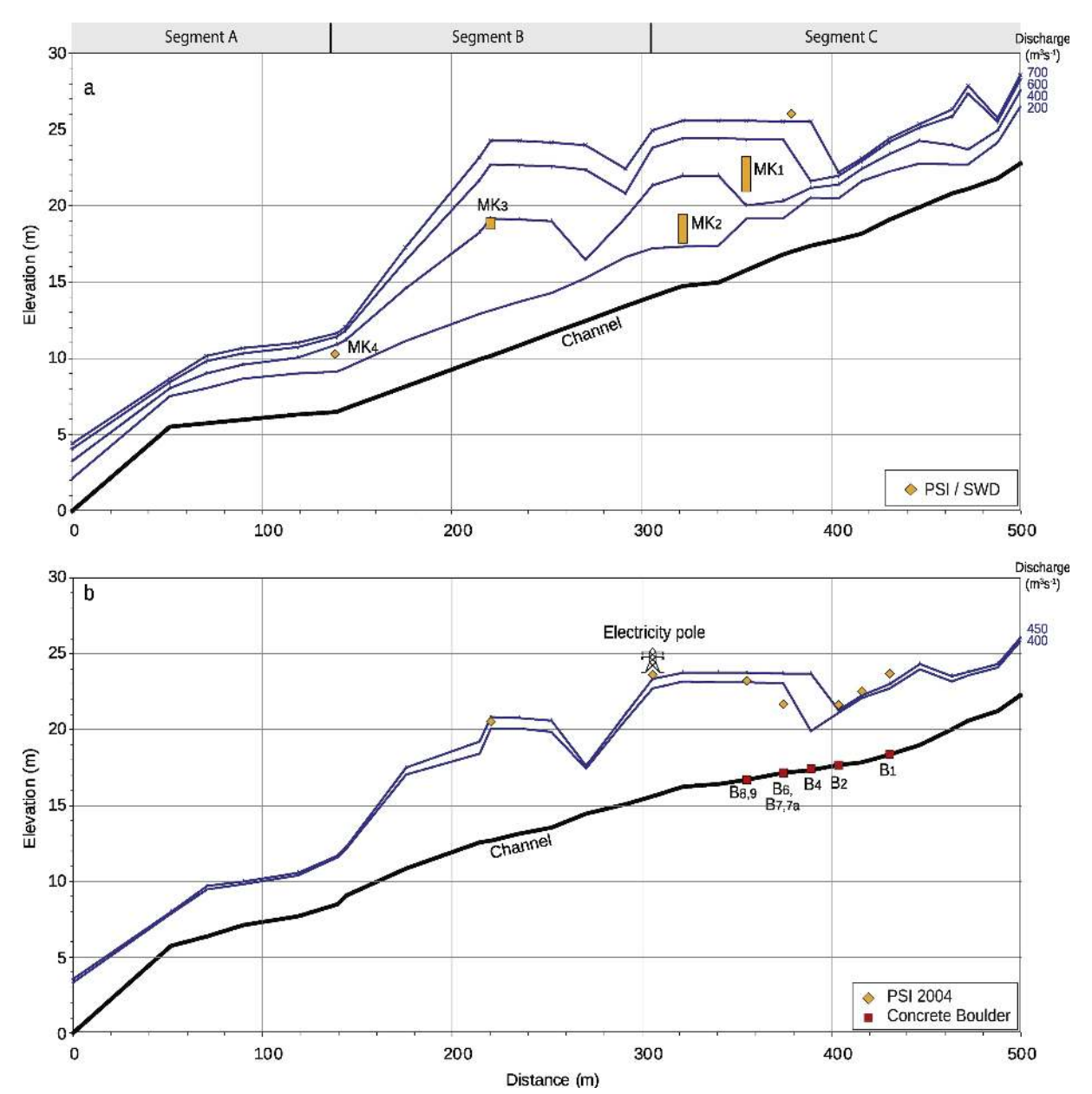
Segment A
Segment B
Segment C
Discharge (m³s⁻¹)
700
600
400
200
a
MK1
MK2
MK3
MK4
Channel
PSI / SWD
Elevation (m)
0
5
10
15
20
25
30
0
100
200
300
400
500
b
Discharge (m³s⁻¹)
450
400
Electricity pole
B8,9
B6, B7,7a
B4
B2
B1
Channel
PSI 2004
Concrete Boulder
Elevation (m)
Distance (m)

Figure 7

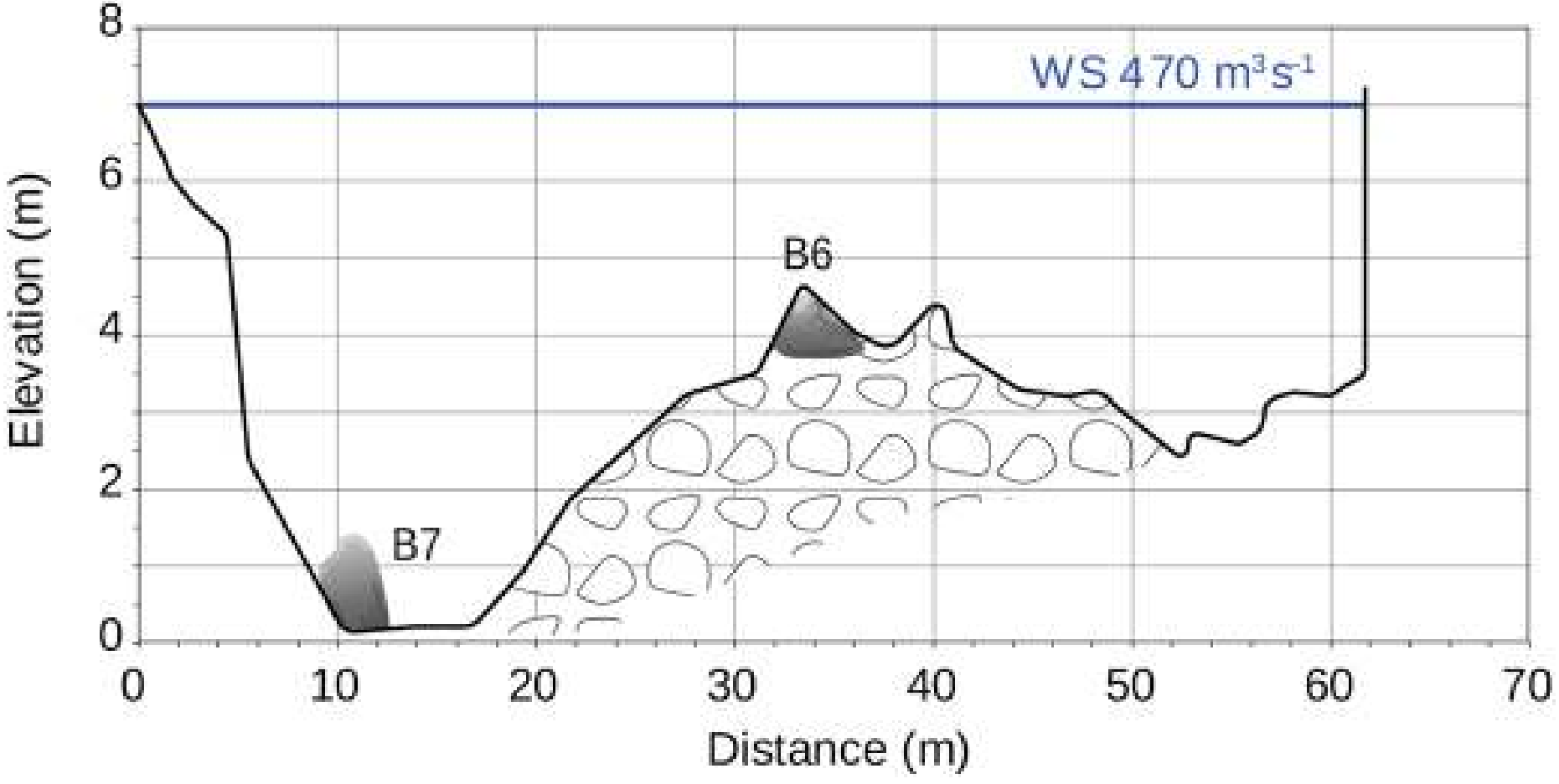
WS 470 m³s⁻¹
B6
B7
Elevation (m)
Distance (m)
0
2
4
6
8
0
10
20
30
40
50
60
70

Figure 8

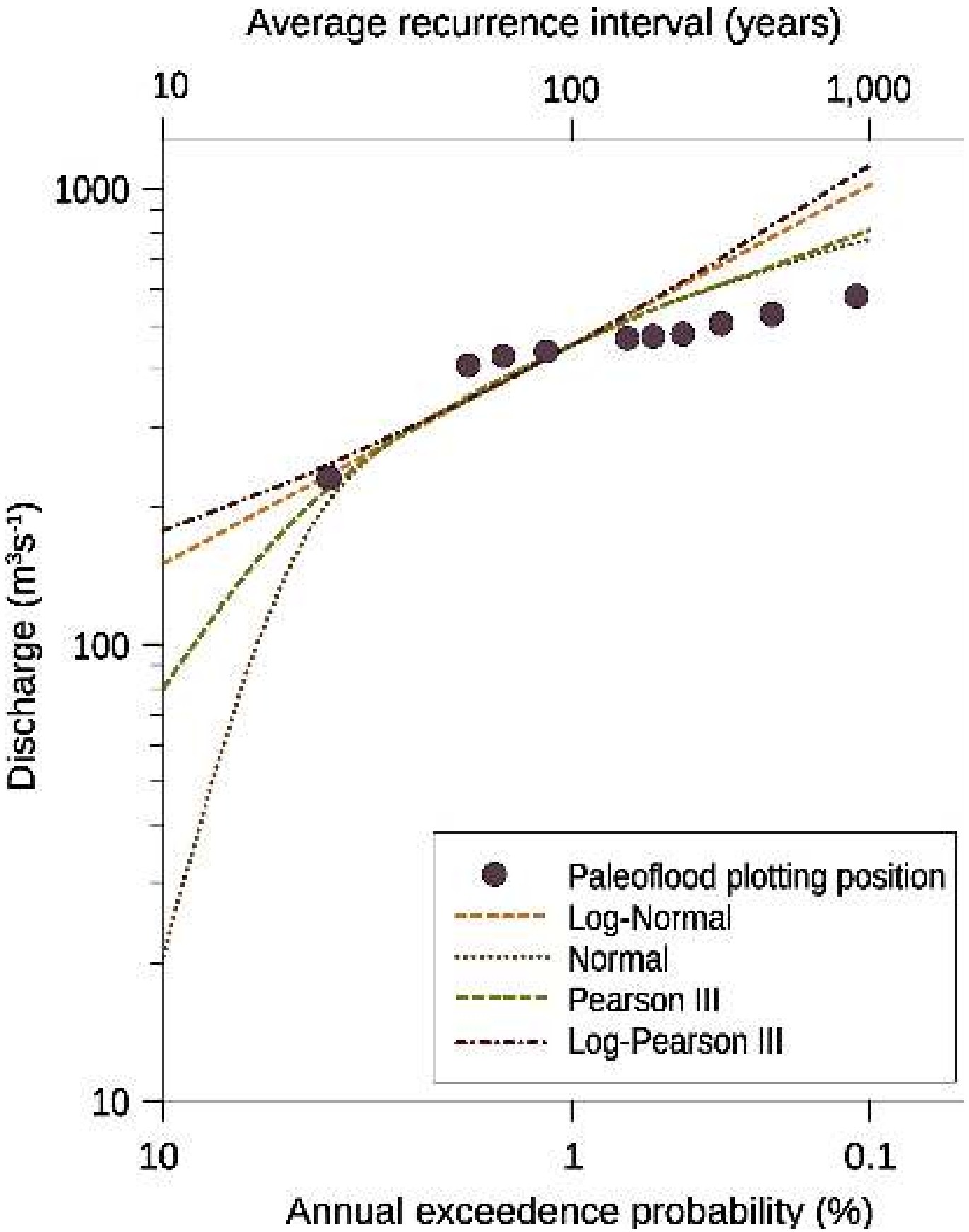
Average recurrence interval (years)
10
100
1,000
1000
100
10
Discharge (m³s⁻¹)
Paleoflood plotting position
Log-Normal
Normal
Pearson III
Log-Pearson III
10
1
0.1
Annual exceedence probability (%)

Figure 9

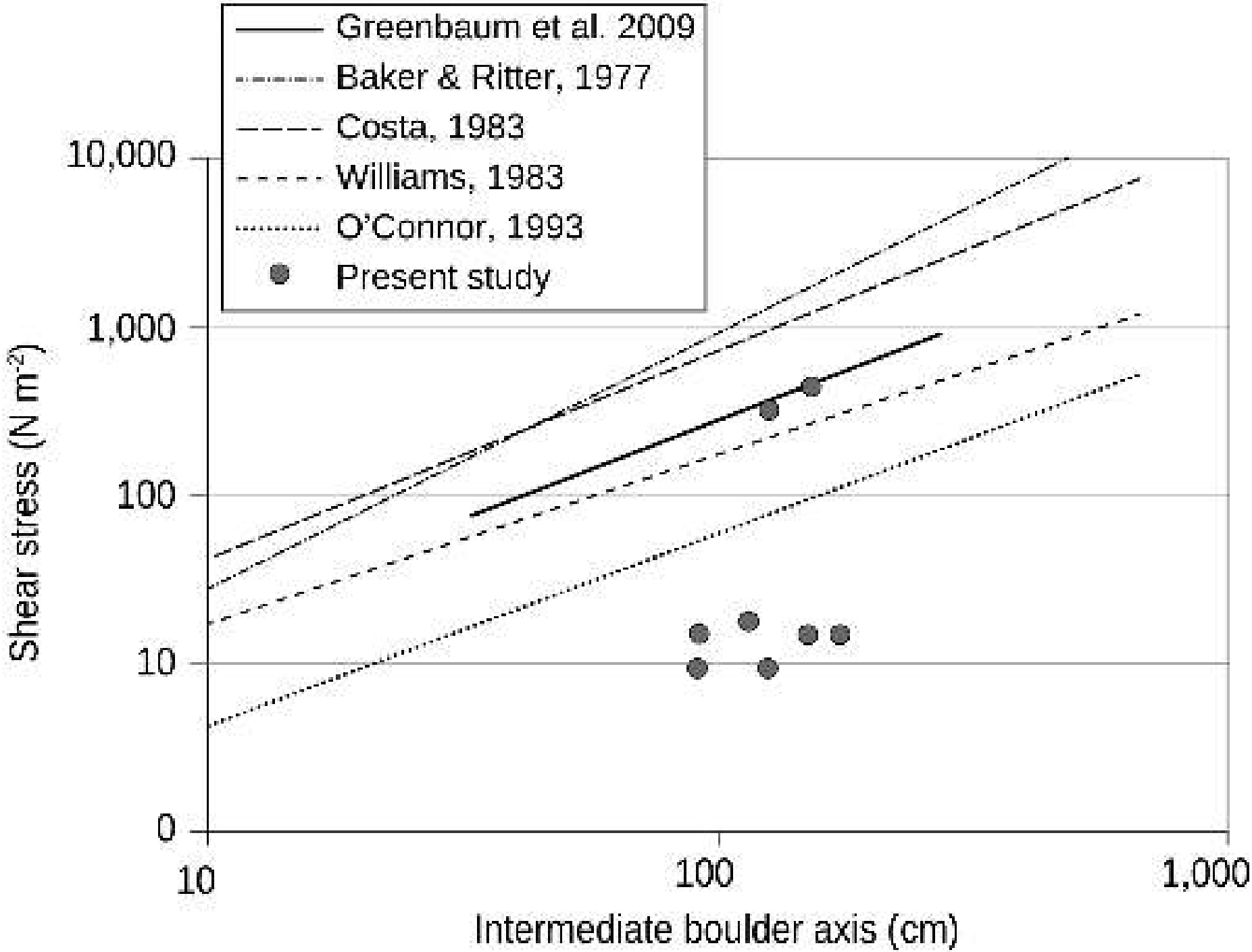
Greenbaum et al. 2009
Baker & Ritter, 1977
Costa, 1983
Williams, 1983
O'Connor, 1993
Present study
10,000
1,000
100
10
0
Shear stress (N m-2)
10
100
1,000
Intermediate boulder axis (cm)

Figure 10